SLC25A46 Promotes Mitochondrial Fission and Mediates Resistance to Lipotoxic Stress in INS-1E Insulin Secreting Cells

Jaime Santo-Domingo[1,2,*], Steve Lassueur[1], Antonio Núñez Galindo[4], Pilar Alvarez-Illera[2], Silvia Romero-Sanz[2], Elena Caldero-Escudero[2], Sergio de la Fuente[3], Loïc Dayon[4,5] and Andreas Wiederkehr[1,5]

[1]Department of Cell Biology, Nestlé Institute of Health Sciences, Nestlé Research, Lausanne, Switzerland
[2]Department of Biochemistry and Molecular Biology, Unidad de Excelencia Instituto de Biología y Genética Molecular (IBGM), Faculty of Medicine, Valladolid, Spain
[3]Center for Translational Medicine, Department of Medicine, Thomas Jefferson University, Philadelphia, PA, 19107, USA
[4]Proteomics, Nestlé Institute of Food Safety & Analytical Sciences, Nestlé Research, Lausanne, Switzerland
[5]Ecole Polytechnique Fédérale de Lausanne, CH-1015 Lausanne, Switzerland

*Corresponding author: Jaime Santo-Domingo
Department of Biochemistry and Molecular Biology. Faculty of Medicine, Unidad de Excelencia Instituto de Biología y Genética Molecular (IBGM), University of Valladolid.
Calle Ramón y Cajal, 7. 47003. Valladolid, Spain
Tel: +34 983184588
E-mail: Jaime.santo-domingo@uva.es

Abstract

Glucose sensing in pancreatic beta-cells depends on oxidative phosphorylation and mitochondria-derived signals that promote insulin secretion. Using mass spectrometry-based phosphoproteomics to search for down-stream effectors of glucose dependent signal transduction in INS-1E insulinoma cells, we identified the outer mitochondrial membrane protein SLC25A46. Under resting glucose concentrations, SLC25A46 was phosphorylated on a pair of threonine residues (T44/T45) and was dephosphorylated in response to glucose-induced calcium signals. Overexpression of SLC25A46 in INS-1E cells caused complete mitochondrial fragmentation, resulting in a mild mitochondrial defect associated with lowered glucose-induced insulin secretion. In contrast, inactivation of the SLC25A46 gene resulted in dramatic mitochondrial hyperfusion but without affecting respiratory activity or insulin secretion. Consequently, SLC25A46 is not essential for metabolism-secretion coupling under normal nutrient conditions. Importantly, insulin secreting cells lacking SLC25A46 had an exacerbated

sensitivity to lipotoxic conditions undergoing massive apoptosis when exposed to palmitate. Therefore, in addition to its role in mitochondrial dynamics, SLC25A46 plays a role in preventing mitochondria-induced apoptosis in INS-E cells exposed to nutrient stress. By protecting mitochondria, SLC25A46 may help to maintain beta-cell mass essential for blood glucose control.

Introduction

Stimulation of pancreatic beta-cells by glucose promotes insulin secretion the hormone which lowers blood glucose following a meal. Beta-cells sense glucose *via* its uptake and metabolism (de Vos et al., 1995; Schuit et al., 1997). Mitochondria are playing an essential role in this process by oxidizing glucose-derived pyruvate. Acute stimulation of beta-cells with glucose enhances mitochondrial CO_2 production, oxygen consumption and mitochondrial ATP synthesis rates as part of the sensing mechanism leading to an adapted insulin secretory response (Antinozzi et al., 2002; de Marchi et al., 2014; Hellman et al., 1974; Santo-Domingo et al., 2019; Wiederkehr & Wollheim, 2012). Mitochondrial metabolism also generates metabolic signals most importantly ATP, which inhibits the plasma membrane K_{ATP} channel. Closure of the K_{ATP} channel depolarizes the beta-cell, which leads to calcium influx through voltage gated calcium channels and the stimulation of exocytosis (Rorsman & Ashcroft, 2018; Wiederkehr & Wollheim, 2012).

Pancreatic beta-cells contain densely packed mitochondria composed of multiple juxtaposed filamentous networks (Molina et al., 2009; Park et al., 2008; Twig et al., 2008). These networks are in constant motion and their filaments undergo continuous remodeling (Griesche et al., 2019; Molina et al., 2009) through the fusion of mitochondria with each other and the fission into shorter mitochondrial units. Mitochondrial fission requires dynamin related protein (DRP1), which binds to outer mitochondrial membrane receptors where it couples GTP hydrolysis to mitochondrial fission. Mitofusins (Mfn1 and Mfn2) and autosomal dominant optic atrophy 1 (OPA1) are the GTPases responsible for mitochondrial fusion (Liesa et al., 2009). Pronounced fragmentation or alternatively mitochondrial swelling in combination with mitochondrial aggregation can be observed following manipulation of proteins of the fission and fusion machineries in beta-cells (Hennings et al., 2018; Molina et al., 2009; Park et al., 2008). The knockout of several fission fusion genes perturbs mitochondrial function and/or glucose-induced insulin secretion (Hennings et al., 2018; Park et al., 2008; Zhang et al., 2011).

Several of these core-shaping proteins also control the ultrastructural organization of mitochondria for example at the level of cristae of the inner mitochondrial membrane (Frezza et al., 2006; Neupert, 2012) and directly or indirectly energy metabolism (Liesa et al., 2009; Park et al., 2008; Pich et al., 2005). OPA1 for example controls cristae junctions to maintain normal inner mitochondrial

membrane compartmentalization (Frezza et al., 2006; Olichon et al., 2003). Consistent with this function, mitochondria in beta-cells lacking OPA1 are short with highly disorganized cristae (Zhang et al., 2011). The OPA1 knockout islets display reduced respiratory chain activity, a poor respiratory response to glucose and fail to secrete insulin *in vivo* resulting in severely impaired glucose tolerance (Zhang et al., 2011). However, aggregation of mitochondria alone is not sufficient to impair energy metabolism and insulin secretion in beta-cells (Hennings et al., 2018; Park et al., 2008).

Proteins of the fission and fusion machineries also play an important role in the regulation of apoptosis (Lee et al., 2004; Liesa et al., 2009). One mechanism linking OPA1 or DRP1 to apoptosis is through the regulation of cristae morphology and the release of apoptogenic factors including cytochrome c in response to cellular stress (Frezza et al., 2006; Germain et al., 2005) . Beta-cells are nutrient sensors but suffer when exposed chronically to elevated glucose or lipids (Eizirik et al., 1992; El-Assaad et al., 2003; Maedler et al., 2001; Molina et al., 2009; Shah et al., 2013). Exposure of beta-cells to lipotoxic conditions causes fragmentation of mitochondria by suppressing their ability to undergo mitochondrial fusion which occurs already before apoptosis is initiated (Molina et al., 2009). Chronic high glucose has only minor effects on mitochondrial morphology although acute glucose stimulation causes transient fragmentation and re-localization of mitochondria in insulin secreting cells (Griesche et al., 2019; Jhun et al., 2013; Molina et al., 2009). Preventing mitochondrial fragmentation (after knockdown of Fis1) protected insulin secreting cells from lipotoxicity-induced apoptosis (Molina et al., 2009) consistent with earlier findings showing that down regulation of Fis1 delays cytochrome c release and apoptosis (Lee et al., 2004).

Dominant optic atrophy and Charcot-Marie-Tooth type 2 are hereditary neurodegenerative disorders frequently caused by mutations in OPA1 or MFN2, respectively. More recently, loss of function mutants of SLC25A46 were found in families with members displaying both optic atrophy and axonal peripheral neuropathy (Abrams et al., 2015). SLC25A46 is an outer mitochondrial membrane protein important for the regulation of mitochondrial fission and the maintenance of mitochondrial cristae structure (Abrams et al., 2015; Janer et al., 2016). These findings establish links between altered mitochondrial dynamics, the control of cristae structure and hereditary neuropathies.

Here we identify SLC25A46 as a mitochondrial phosphoprotein and important regulator of mitochondrial dynamics in insulin secreting beta-cells. SLC25A46 is phosphorylated on threonine T44 and T45. During acute glucose stimulation, SLC25A46 is dephosphorylated in a calcineurin dependent manner. Phosphoregulation modulates the effect of SLC25A46 on mitochondrial dynamics. Disruption of SLC25A46 in INS-1E insulinoma cells causes pronounced hyperfilamentation of mitochondria, while mitochondrial respiration and glucose-induced insulin secretion are preserved. Importantly, lack of SLC25A46 function sensitizes the insulin secreting cells to lipotoxicity.

Results

Glucose-dependent SLC25A46 phosphorylation in INS-1E insulinoma cells

Through the analysis of the phosphoproteome in the INS-1E rat insulin secreting cell line, we have previously described glucose dependent protein phosphorylation and dephosphorylation events involved in biological processes ranging from insulin biosynthesis, vesicle trafficking to insulin granule exocytosis and cytoskeleton remodeling (Santo-Domingo et al., 2019) consistent with several related studies with insulinoma cells and primary beta-cells. Our experimental setup was to follow glucose dependent phosphorylation changes over three time-points (5, 30 and 60 minutes) in the presence of maximal stimulatory glucose (16.7 mM) and compare the phosphoproteome to the one of INS-1E cells maintained for the same duration under resting glucose conditions (2.5 mM). Following new analysis of the data (see Material and Methods), we identified herein 37 additional mitochondrial peptides (sometimes containing multiple serines and/or threonines) with putative phosphorylation site(s) but where the exact localization of the modification(s) was still uncertain (Fig. 1A; Suppl. Table 1-3). The strongest glucose-induced fold change was observed for a 22 amino acid-long di-phosphorylated peptide within the mitochondrial membrane protein SLC25A46 (Fig. 1B). This study thus focuses on the glucose-dependent regulation of SLC25A46 and the role of this protein in the control of mitochondrial function during stimulus secretion coupling in INS-1E cells.

SLC25A46 has 6 predicted transmembrane domains similar to other members of the SLC25 family of mitochondrial carriers. The phosphopeptide identified here is localized on the N-terminal domain flanking the first transmembrane domain of SLC25A46 (Fig. 1B). The identified peptide contains 6 potential phosphorylation sites. Serines and threonines in this sequence are conserved between mammalian species. The pair of threonines (T44/T45) on SLC25A46 is even conserved with more distant species including chicken, frog and zebrafish (Fig. 1B).

After stimulation of INS-1E cells with 16.7 mM glucose, phosphorylation of this phosphopeptide was reduced compared to control cells maintained in basal (2.5 mM) glucose (Fig. 1C). In this respect, phosphorylation changes in this peptide behaved similarly to the autophosphorylation site S108 on the β-subunit of the energy sensor AMPK (Fig. 1D).

Based on the proteomic data, the highest probability of phosphorylation localizations was assigned automatically by the Scaffold PTM software to S35 and T45, concomitantly, but still with a very limited confidence (*i.e.*, 40%). Manual inspection of tandem mass spectra revealed in fact inconclusive for localization of the phosphorylation modifications on S35 or T37 one side and T44 or T45 on the other side. To validate T45 and the neighboring T44 as sites of glucose-dependent phosphorylation, we raised polyclonal antibodies against SLC25A46 peptides phosphorylated on T44 and T45 (see Materials and Methods). The antibodies recognized a protein of about 46 kDa (Fig. 1E)

consistent with the predicted size of SLC25A46 (Fig. 1E-F) and the detection of the same size band with a commercial antibody raised against SLC25A46 (Fig. 1G). The Western signals were lost after λ-phosphatase treatment of INS-1E lysates (Fig. 1E) demonstrating our antibodies recognize the phosphorylated form of SLC25A46. Furthermore, our phospho-specific antibodies recognized a DDK tagged SLC25A46 protein (SLC25A46-DDK) but failed to detect the phospho-null mutant (SLC25A46 A44/A45-DDK) when these transgenes were expressed in INS-1E cells. The commercial SLC25A46 antibody recognized both exogenously expressed wild-type and phosphorylation mutant proteins (Fig. 1G). Jointly, these findings showed that our antibodies recognize the phosphorylated SLC25A46 epitope.

Western blotting using the phosphorylation specific antibodies confirmed that glucose levels strongly affected the phosphorylation status of SLC25A46 on T44/T45 as already suggested by our mass spectrometry results. The phosphorylation status of T44/T45 of SLC25A46 increased with time (5-60 minutes) when INS-1E cells were transferred from culture medium (11 mM glucose) to a sub-stimulatory glucose concentration (2.5 mM). This increase was strongly attenuated in glucose stimulated (16.7 mM) INS-1E cells (Fig. 1F). We concluded, the phosphorylation status of SLC25A46 on T44/T45 is regulated by glucose-induced signal transduction. SLC25A46 phosphorylation is maximal in resting INS-1E cells whereas stimulatory glucose promotes dephosphorylation of the protein.

Glucose-driven SLC25A46 T44/T45 dephosphorylation is mediated by Calcineurin

In silico searches (NetPhos 3.1) did not reveal any high confidence kinase substrate consensus motif sequence around the T44/T45 phosphorylation site (data not shown). Given the close correlation between glucose induced $AMPK_{S108}$ and $SLC25A46_{T44/T45}$ dephosphorylation kinetics (Fig. 1C-D), we tested whether energy stress is responsible for the observed elevated phosphorylation under sub-stimulatory glucose concentrations. We find that respiratory chain inhibitors and uncouplers known to activate AMPK decreased rather than increased the phosphorylation status of SLC25A46 (Fig. 2A). In addition, direct activation of AMPK with AICAR had no effect on SLC25A46 phosphorylation (Fig. 2A). Furthermore, pharmacological stimulation with 991 activated AMPK (phosphorylation of Threonine T172) without modifying the phosphorylation status of $SLC25A46_{T44/T45}$ in low glucose conditions nor preventing its glucose-induced dephosphorylation (Fig. 2B). Collectively, we conclude that AMPK activity does not influence glucose dependent $SLC25A46_{T44/T45}$ phosphorylation.

Interestingly, removal of extracellular Ca^{2+} to prevent glucose-dependent Ca^{2+} influx blocked glucose-dependent $SLC25A46_{T44/45}$ dephosphorylation (Fig. 2C) suggesting the involvement of a Ca^{2+}sensitive kinase or phosphatase. A candidate calcium regulated phosphatase affecting beta-cell function is calcineurin. The two calcineurin inhibitors CsA (Fig. 2E-G) and FK506 (Fig. 2D-F) partially inhibited

glucose induced SLC25A46$_{T44/T45}$ dephosphorylation both at 30 and 60 minutes. Quantification of 4 independent experiments show that on average both inhibitors counteract glucose-induced phosphorylation (Fig. 2F, G). Due to the variability between experiments statistical significance was reached only for the condition where CsA was used for 60 minutes. For the shorter time-point or the FK506 treatment only a trend to inhibit glucose dependent phosphorylation was observed. These findings suggest the Ca^{2+}-sensitive phosphatase calcineurin may be involved in glucose dependent regulation of SLC25A46$_{T44/T45}$. In parallel, we followed Ser S637 phosphorylation of Drp1 a well-characterized calcineurin substrate. Glucose stimulation failed to induce Drp1$_{S637}$ dephosphorylation. However, both calcineurin inhibitors enhanced Drp1$_{S637}$ phosphorylation, confirming effective pharmacological inhibition of calcineurin in these experiments (Fig. 2D, E; quantification in Suppl. Fig. 1A, B).

SLC25A46 overexpression lowers glucose-induced respiration and insulin secretion

Next, we assessed the impact of SLC25A46 on mitochondrial function and its role in metabolism-secretion coupling. To this end, we disrupted SLC25A46 in INS-1E cells by Crispr/Cas9 gene targeting. Successful disruption of the SLC25A46 alleles in individual clones was confirmed by sequencing (Suppl Fig. 2). At the protein level, SLC25A46 expression was either dramatically reduced or completely absent (Fig. 3A).

The SLC25A46 deficient cell lines had no consistent respiratory defect (Fig. 3B-D). Basal respiration (Fig. 3C) and oligomycin dependent respiration after glucose stimulation were close to normal (Fig. 3D). Glucose and KCl-induced cytosolic calcium signaling was indistinguishable between SLC25A46 deficient and wild-type INS-1E cells (Fig. 3E-F). Characterization of SLC25A46 deficient cells revealed clone specific differences in insulin content (Fig. 3G) but insulin secretion when expressed per insulin content was close to normal. Fold glucose-stimulated insulin secretion was similar in wild-type and SLC25A46 deficient INS-1E clones (Fig. 3H). These findings showed that disruption of the SLC25A46 gene does not markedly affect metabolism-secretion coupling in INS-1E cells.

We next tested whether overexpression of SLC25A46 had an impact on metabolism-secretion coupling. Overexpression in INS-1E cells was achieved by infecting cells with an adenovirus carrying a DDK tagged SLC25A46 expressed under the control of the CMV promoter (Ad-CMV-SLC25A46-DDK). Dependent on the Ad-CMV-SLC25A46-DDK titer, we obtained INS-1E cells expressing SLC25A46-DDK protein several fold over the endogenous SLC25A46 protein levels (Fig. 3I). SLC25A46 overexpression reduced basal respiration and the oligomycin dependent fraction of glucose-induced respiration compared to control Ad-CMV-luciferase infected cells, (Fig. 3J, K, L). In agreement with the respiratory defect observed, glucose-induced cytosolic calcium signaling was significantly diminished in SLC25A46-DDK overexpressing cells (Fig. 3M-N). SLC25A46-DDK

overexpression did not affect the insulin content but significantly lowered glucose-stimulated insulin secretion (Fig. 3 O-P). We concluded that enhanced SLC25A46 function partially disrupts metabolism-secretion coupling in INS-1E cells.

SLC25A46 regulates mitochondrial dynamics in pancreatic beta cells

In agreement with earlier publications, we found SLC25A46 localizes to mitochondria. After differential centrifugation, SLC25A46 was enriched in the mitochondrial fraction together with TOM20 a subunit of the mitochondrial protein import machinery (Fig. 4A). In addition, we observed co-localization of SLC25A46-GFP with the mitochondrial membrane potential sensor TMRM (Fig. 4B). TMRM staining also revealed that mitochondria in INS-1E cells expressing SLC25A46-GFP were more fragmented (Fig. 4B, right panel) than neighboring non-transfected control cells. This effect on mitochondrial morphology is consistent with earlier reports that demonstrate SLC25A46 promotes mitochondrial fission (Abrams et al., 2015). We therefore tested whether manipulation of SLC25A46 expression affects mitochondrial network dynamics in insulin secreting cells. Mitochondrial morphology was inspected in control INS-1E, SLC25A46 deficient and SLC25A46 overexpressing cells and classified as hyperfused, intermediate, or fragmented (Fig. 4C). In SLC25A46 deficient cells, the fraction of cells with hyperfused mitochondria was strongly increased (Fig. 4C). In INS-1E cells overexpressing SLC25A46 almost no hyperfused mitochondria were detected and a fragmented mitochondrial phenotype was observed in the majority of cells (Fig. 4C).

Mitochondrial dynamics in INS-1E cells was also studied quantitatively by fluorescence recovery after photo-bleaching (FRAP) using a mitochondrial matrix targeted RFP (Fig. 4D). FRAP kinetics is known to be faster in hyperfused mitochondrial networks where recovery is rapid due to the refilling of the matrix space by RFP protein diffusion from neighboring unbleached mitochondrial filaments (Fig. 4E). When the mitochondrial network is fragmented recovery of fluorescence is slower. SLC25A46 deficiency promoted faster and more substantial recovery after photo bleaching (Fig. 4E-F), while overexpression of SLC25A46 precluded efficient recovery (Fig. 4E-F). Both deletion and over-expression of SLC25A46 had dramatic effects on mitochondrial morphology in INS-1E cells (Fig. 4G). Qualitative assessment of electron microscopy images did not reveal any striking phenotype beyond a slight enlargement of SLC25A46 deficient mitochondria, with no apparent effect on cristae number, density or organization in cells lacking or overexpressing SLC25A46 (Fig. 4H).

The molecular mechanism engaged by SLC25A46 to control the mitochondrial network remains poorly understood. We therefore tested whether manipulation SLC25A46 protein levels affected protein levels of well-known factors of the core mitochondrial fission fusion machinery. We find protein expression of L-Opa1, S-Opa1, Drp1 and Mfn2 in SLC25A46 deficient (Fig. 4I) and overexpressing cells (Fig. 4I) normal compared to control INS-1E cells. Interestingly, Mfn1 protein

levels slightly increased in SLC25A46 deficient INS-1E cells (Fig. 4I). These findings are consistent with the earlier findings showing that pro-fusion protein Mfn1 is stabilized in cells lacking SLC25A46 (Steffen et al., 2017). Furthermore, Drp1 S637 phosphorylation status decreased in SLC25A46 deficient INS-1E cells (Fig. 4I).

T44/T45 phosphorylation inhibits SLC25A46 mediated mitochondrial fragmentation

We next evaluated whether T44/T45 phosphorylation regulated the ability of SLC25A46 to alter mitochondrial network dynamics. To this end, wild-type SLC25A46 and a double phosphorylation deficient mutant SLC25A46 T44A/T45A (Fig. 5A) were cloned under the control of a doxycycline-inducible promoter and transfected into INS-1E clones lacking endogenous SLC25A46 expression. In these cells, SLC25A46 expression was strictly doxycycline-dependent (Fig. 5B). Close to maximal expression was achieved with 10 ng/ml of doxycycline in the medium for both the wild-type and phospho-deficient mutant protein (Fig. 5B). Glucose dependent dephosphorylation was preserved in cells expressing the transgene under the control of the deoxycycline-inducible promoter. As expected, the phosphoantibody did not recognize the SLC25A46 T44A/T45A mutant protein (Fig. 5B). Mitochondrial dynamics was further quantified by FRAP analysis of mitochondrial matrix targeted RFP. Recovery after photobleaching was very rapid in the filamentous mitochondria of SLC25A46 deficient INS-1E cells (Fig. 5C-D). Consistent with its pro-fission properties, doxycycline-induced expression of the wild-type protein in SLC25A46 deficient cells caused fragmentation of the mitochondrial network, slowed recovery in FRAP experiments (Fig. 5C) and provided a less pronounced recovery of the initial signal before photobleaching (Fig. 5D). Expression of the T44A/T45A phosphorylation deficient mutant resulted in an intermediate phenotype (Fig. 5D-E). Fragmentation was less pronounced and FRAP was accelerated compared to cells expressing the SLC25A46 wild-type protein (Fig. 5C-D). We concluded, phosphorylation of T44/T45 is required for maximal pro-fission activity of SLC25A46 and proposed that T44/T45 phosphorylation regulates SLC25A46 function.

Considering the significant effect of SLC25A46 deficiency on Mfn1 levels and Drp1 S637 phosphorylation status, we further explored whether the pro-fusion properties of the phosphorylation deficient mutant SLC25A46 T44A/T45A is concomitant with changes on these proteins. However, reintroduction of either wild-type or double phosphorylation deficient mutant SLC25A46 T44A/T45A variants in SLC25A46 deficient cells did neither modify the Mfn1 levels nor the Drp1 S637 phosphorylation status (Suppl. Fig. 3).

SLC25A46 KO prevents palmitate-induced fragmentation but sensitizes INS-1E cells to palmitate-induced apoptosis

Shifting the balance towards mitochondrial fusion has been found previously to protect pancreatic β-cells from nutrient overload induced cell death (Molina et al., 2009). Consistent with this previous report, we observed massive mitochondrial fragmentation following acute palmitate (200 μM) stimulation of INS-1E cells (Fig. 6A). In SLC25A46 deficient cells, mitochondrial morphology underwent palmitate induced qualitative changes, but mitochondria remained mostly hyperfused (Fig. 6A-B). Palmitate-induced fragmentation slowed the kinetics of FRAP in wild-type and SLC25A46 deficient cells. In the SLC25A46 deficient cells, FRAP remained more rapid even in palmitate treated cells when compared to wild-type cells under control nutrient conditions (Fig. 6B). These FRAP results are consistent with the well preserved filamentous mitochondrial network of SLC25A46 deficient cells even after treatment with palmitate (Fig. 6A-B). We therefore tested whether in a similar manner prevention of mitochondrial fragmentation in SLC25A46 deficient cells may protect from palmitate-induced apoptosis. Cell death was followed continuously by surface labeling with Annexin V. During apoptosis, phosphatidylserine molecules translocate to the outer leaflet of the plasma membrane, which can then be detected with fluorescently labeled Annexin V (see Materials and Methods). Exposure of control INS-1E cells to palmitate induced a gradual increase in apoptosis beyond 24 hours of incubation in the presence 200 μM of the fatty acid. Apoptosis was highly exacerbated in SLC25A46 deficient cells (Fig. 6C). Dose- response experiments confirmed SLC25A46 deficient cells were more sensitive to palmitate induced apoptosis over a range of palmitate concentrations (Fig. 6D). We found that insulin secreting cells lacking SLC25A46 preserve a filamentous mitochondrial network when challenged with palmitate. However, this ability to prevent mitochondrial fragmentation does not protect from palmitate-induced apoptosis. On the contrary, INS-1E cells deficient for SLC25A46 are much more sensitive to the harmful effects of palmitate stress.

To further explore the potential cellular mechanisms mediating the higher sensitivity of SLC25A46 deficient cells to palmitate-induced apoptosis, and considering previous studies reporting altered mitochondrial lipid homeostasis (Janer et al., 2016), we hypothesized that sensitivity of SLC25A46 deficient cells to palmitate-induced apoptosis may be caused by inefficient oxidation of fatty acids. To test this possibility, we measured palmitate-induced mitochondrial respiration in wild type and SLC25A46 deficient cells (Fig. 6E). We did not find differences in the ability of SLC25A46 deficient cells and control cells to oxidize palmitate.

Lipid peroxidation plays a critical role in apoptotic cell death. We therefore tested whether lipid peroxidation was altered in cells lacking SLC25A46 expression. We observed that lipid peroxidation was not significantly different between wild-type and SLC25A46 knockout INS-1E cells (Fig. 6F).

Palmitate treatment caused a marked reduction of lipid peroxidation in INS-1E control and knockout cells. The observed difference in apoptosis is therefore not due to differences in lipid peroxidation.

Considering the higher sensitivity of SLC25A46 deficient cells to palmitate-induced apoptosis, we tested whether the SLC25A46 44T/45T phosphorylation status alters the sensitivity of INS-1E cells to undergo nutrient-driven apoptosis. Neither overexpression of wild-type SLC25A46 nor SLC25A46 phosphorylation mutant (T44/45A) was able to prevent palmitate-induced apoptosis in INS-1E cells (Fig. 6G). We conclude that physiological levels of the SLC25A46 protein are required to protect INS-1E cells from palmitate stress. Furthermore, we tested whether similar to glucose palmitate was able to modify the phosphorylation status of SLC25A46. We observe that SLC25A46 levels and T44/45 phosphorylation status remained unchanged after acute or chronic incubation with 200µM palmitate (Suppl. Fig. 4A-B). Changes in SLC25A46 T44/45 phosphorylation are not required for palmitate to induce INS-1E cell apoptosis.

Discussion

SLC25A46 was discovered a few years ago as mutated in individuals with a novel form of mitochondrial disease primarily affecting neuronal tissues. Neuronal defects associated with SLC25A46 loss of function include peripheral neuropathy, optic atrophy and cerebellar ataxia. Unlike, most other mitochondrial membrane proteins of the SLC25 family, SLC25A46 localizes to the outer mitochondrial where it may act as a functional homologue of Ugo1p, which coordinates the fusion of the inner and outer mitochondrial membrane in yeast (Abrams et al., 2015; Sesaki & Jensen, 2004). In addition, SLC25A46 like Ugo1p interacts both with OPA1 and mitofusin (Janer et al., 2016). Such protein-protein interaction and the shared phenotype of SLC25A46 and Opa1 mutations to cause optic atrophy strongly suggest a main function of SLC25A46 in the control of mitochondrial morphology. However, earlier findings indicate multiple additional functions of SLC25A46 at the interface between the outer and inner mitochondrial membrane. SLC25A46 binds to proteins of the MICOS complex, which controls mitochondrial inner membrane architecture (Kozjak-Pavlovic, 2017; Neupert, 2012). As a result, impaired SLC25A46 function perturbs cristae morphology and reduces respiration (Abrams et al., 2015; Janer et al., 2016). Furthermore, SLC25A46 appears to play an important role in the exchange of phospholipids between the endoplasmic reticulum and mitochondria (Janer et al., 2016). Today many open questions regarding the molecular function of SLC25A46 remain.

We identified SLC25A46 as a phosphoprotein during a search for down-stream effectors of glucose signaling in beta cells. Glucose dependent phosphorylation occurs on the N-terminus in a peptide sequence preceding the first of the 6 transmembrane domains. Using antibodies specifically

recognizing the phosphorylated epitope, we could confirm glucose dependent phosphorylation of a central pair of threonine residues (T44/T45) on this protein. SLC25A46 T44/T45 phosphorylation was most pronounced when INS-1E cells were kept under resting glucose conditions. Stimulatory glucose concentrations strongly reduced SLC25A46 T44/T45 phosphorylation. It is worth mentioning that the phosphorylation status of SLC25A46 T44/T45 slightly increased overtime regardless of glucose levels (see the time-course under low glucose conditions, and under stimulatory glucose conditions, Fig. 1F). This is probably reflecting the activity of phosphorylation pathways that still adapts to the switch from regular cell culture medium to KRBH, and suggest that the phosphorylation status of SLC25A46 T44/T45 is additionally controlled by glucose-independent mechanisms.

The localization of SLC25A46 in the outer mitochondrial membrane (Abrams et al., 2015; Janer et al., 2016) renders this protein accessible to cytosolic kinases and phosphatases. Exposure of the N-terminus to the cytosol has not yet been demonstrated experimentally but was inferred from sequence comparison with two other SLC25 family members on the outer mitochondrial membrane (Palmieri, 2013; Ruprecht & Kunji, 2020; Sesaki & Jensen, 2001). We propose that SLC25A46 is a sensor of glucose-dependent signal transduction residing on the outer mitochondrial membrane in pancreatic beta-cells. Given the essential roles mitochondria play in beta-cell nutrient sensing and insulin secretion, a role for SLC25A46 in beta-cell function or health is likely.

The SLC25A46 amino acids surrounding T44 and T45 does not contain any typical kinase consensus sequence and we have failed to identify upstream kinases responsible for SLC25A46 phosphorylation. On the other hand, we noted that blocking glucose-induced calcium rises in INS-1E cells prevented glucose dependent dephosphorylation of T44/T45. We find that the two calcineurin inhibitors CsA and FK506 blocked glucose-dependent dephosphorylation of SLC25A46 consistent with earlier reports that provide strong evidence for activation of this calcium activated phosphatase during glucose stimulation (Jansson et al., 2008; Screaton et al., 2004). Of note, the calcineurin substrate Drp1 (S637) was also hyperphosphorylated in the presence of either calcineurin inhibitor. In contrast to SLC25A46, Drp1 was dephosphorylated in both at low and high glucose levels. Glucose dependent calcium rises are therefore unlikely to affect Drp1 S637 phosphorylation and the control of mitochondrial fission *via* Drp1 in beta cells. Our results on SLC25A46 suggest that in addition to the important role of calcineurin in linking glucose levels to proliferation and survival of beta cells through TORC2 and NFAT2 dephosphorylation (Heit et al., 2006; Jansson et al., 2008; Screaton et al., 2004), calcineurin may directly influence mitochondrial function by dephosphorylating SLC25A46. We establish a new link between cytosolic calcium signaling and the regulation of beta-cell mitochondria.

Mitochondria in beta-cells participate actively in nutrient sensing and generate coupling factors, most importantly ATP, that regulate insulin secretion. In INS-1E cells lacking SLC25A46, neither the basal

respiratory rate of oxygen consumption nor the biphasic rise of glucose-dependent respiration was altered. Consistent with normal oxidative phosphorylation, our ultrastructural study of mitochondria reveals no apparent disorganization of cristae in the inner mitochondrial membrane.

The lack of respiratory phenotype in mutant insulin secreting cells is diametrically opposite to the pronounced oxidative phosphorylation defect observed in SLC25A46 mutant neurons or patient fibroblasts carrying SLC25A46 mutations (Abrams et al., 2015; Janer et al., 2016; Wan et al., 2016). In these cell types, the absence of SLC25A46 function also causes pronounced alterations of mitochondrial ultrastructure most importantly a disruption of cristae organization. Of note, we identify significant variability in the respiratory activity of the different clones (Fig. 3). We cannot rule out off targeting edition events in our Crispr/Cas edited cell clones, as the genomes of the 3 clones were not fully sequenced.

Glucose-induced cytosolic calcium signaling was normal in INS-1E SLC25A46 KO cells as well. This is another strong argument for close to normal respiratory function. Strong impairment of mitochondria respiration such as observed in mutant neurons and fibroblasts would have prevented glucose-induced ATP production and consequently calcium influx linked to plasma membrane electrical activity in beta-cells. Given the normal cytosolic calcium signals, it is not surprising that also glucose-induced insulin secretion was preserved in SLC25A46 mutant INS-1E cells. We propose that mitochondria in INS-1E express proteins compensating for the loss of SLC25A46 function.

Based on our findings in INS-1E knockout cells, we cannot rule out that SLC25A46 dysfunction impacts oxidative phosphorylation and thereby metabolism secretion coupling in primary pancreatic beta-cells. Indeed, a possible role for SLC25A46 in primary beta cells *in vivo* has recently been suggested through the careful genetic and phenotypic analysis of the insulin hyposecretion mouse (ihs) (Nakano et al., 2020). The authors identified, *Slc25A46* as one of a small group of genes that could be responsible for the described severe insulin secretion defect in these mice.

We demonstrate mild mitochondrial impairment in insulin secreting cells overexpressing SLC25A46. Both basal respiration and ATP-synthase dependent respiration was reduced in cells overexpressing the transgene. The mitochondrial defect in these cells is likely responsible for the strongly impaired cytosolic calcium signaling and the observed reduced glucose-induced insulin secretion. We conclude, SLC25A46 overexpression interferes with the endogenous protein carrying out its function. A possible mechanistic explanation is that SLC25A46 when overexpressed titrates out some of its interaction partners preventing their normal assembly into functional units. Such a dominant negative effect may also be experienced in cells expressing point mutations of SLC25A46 in cells from individuals with mitochondrial disease.

In pancreatic beta-cells, mitochondria form a dense cortical filamentous network in close proximity with the plasma membrane. Mitochondria are therefore positioned strategically to sense glucose-

induced calcium influx and locally generate coupling factors close to insulin granule to promote their mobilization and exocytosis. Mitochondrial filaments in INS-1E and primary beta-cells on average are rather short and highly dynamic. The most striking phenotype of SLC25A46 knockout INS-1E cells is the dramatic elongation of mitochondrial filaments. The mitochondrial filamentation phenotype in INS-1E cells lacking SLC25A46 is consistent with earlier findings in other cell types (Abrams et al., 2015; Janer et al., 2016; Wan et al., 2016). Surprisingly, the pronounced hyperfusion of mitochondria does not affect metabolism secretion coupling as discussed earlier. This is in contrast to the hyper-fusion caused by lack of Drp1 in beta cells, which consistently impairs glucose-induced insulin secretion *in vitro* and *in vivo* (Hennings et al., 2018; Kabra et al., 2017; Reinhardt et al., 2016).

SLC25A46 overexpression in INS-1E cells, induced massive mitochondrial fragmentation in agreement with earlier findings in fibroblasts, neurons and Hela cells (Abrams et al., 2015; Janer et al., 2016; Wan et al., 2016). The results suggest SLC25A46 contributes as a pro-fission factor to mitochondrial dynamics, but the underlying molecular mechanisms remain elusive. In fibroblasts, it was shown that SLC25A46 interacts with Mfn1, Mfn2 and Opa1 core components of the mitochondrial fission machinery (Janer et al., 2016). Later, it was proposed that absence of SLC25A46 stabilized Mfn1 and Mfn2 levels as well as their mutual interaction, favoring pro-fusion (Steffen J, 2016). In agreement with these findings, we observe that SLC25A46 deficiency slightly increased Mfn1 levels. However, overexpression of SLC25A46 did not modify Mfn1 levels nor the abundance of other mitochondrial shaping factor tested despite the robust fragmentation phenotype. We predict the existence of additional factors mediating the pro-fission properties of SLC25A46 beyond the regulation of Mfn1/2 stability.

The massive mitochondrial fragmentation observed in SLC25A46 overexpressing insulinoma cells may explain why SLC25A46 has dominant negative effects on mitochondrial respiration and glucose-induced insulin secretion. These findings are consistent with earlier work. Pancreatic beta-cells lacking the mitochondrial fusion proteins Opa1, Mfn1 or Mfn2 also have strongly fragmented mitochondria and impaired glucose-induced insulin secretion (Zhang et al., 2011). Massive fragmentation may be incompatible with normal metabolism secretion coupling. Proper localization of cortical mitochondria and the regulation of mitochondrial morphology likely influence effective coupling between glucose sensing and the control of insulin secretion. Phosphorylation of SLC25A46 may influence these processes by altering mitochondrial morphology and positioning.

We tested whether the regulation of SLC25A46 phosphorylation on T44 and T45 has functional consequences. Expression of a SLC25A46 alanine mutant (T44A/T45A) that cannot be phosphorylated was much less efficient at causing mitochondrial fragmentation than expression of the corresponding wild-type protein. These findings suggest SLC25A46 phosphorylation stimulates fission activity. Calcium dependent SLC25A46 dephosphorylation would therefore predict a shift to

more elongated mitochondria during glucose stimulation. However, we and others have not observed acute glucose-induced mitochondrial elongation in INS-1E or primary beta cells (data not shown; (Jhun et al., 2013; Molina et al., 2009)). Earlier work by Shirihai and colleagues demonstrated that neither acute nor chronic rises in glucose had a significant impact on mitochondrial morphology in insulin secreting cells. These findings are incompatible with the promotion of mitochondrial fusion caused by glucose associated calcium rises and the dephosphorylation of SLC25A46.

Interestingly, Molina *et al.* found pronounced mitochondrial fission in response to palmitate or a combination of elevated glucose and palmitate. Such lipotoxic conditions have been used to mimic a diabetogenic environment to study the stressed pancreatic beta-cell. The authors further observed that slowing fission by knocking down Fis1 prevented palmitate-induced fragmentation and importantly almost completely blocked palmitate-induced apoptosis (Molina et al., 2009). Knocking out the fission factor SLC25A46 in INS-1E cells similarly almost completely prevented palmitate-induced fragmentation. This mechanism of blocking mitochondrial fragmentation however did not protect INS-1E cells from palmitate-induced apoptosis. On the contrary, SLC25A46 knockout cells were much more sensitive to the toxic effects of palmitate at all concentrations tested. These observations may be linked to the altered mitochondrial phospho-lipidome reported in SLC2546 deficient cells (Janer et al., 2016), given the modulatory effects of mitochondrial membrane lipids on mitochondrial-driven apoptosis. We conclude that maintaining the mitochondrial filamentous network is not sufficient to protect beta-cells from lipotoxicity-induced apoptosis. More importantly, these findings suggest a crucial role for SLC25A46 in the control of mitochondria-induced apoptosis in beta-cells.

The demonstrated role of SLC25A46 in cristae morphology in other cell types could be linked to the control of apoptosis by SLC25A46. In beta cells, this role for SLC25A46 in cristae morphology and function may be compensated under normal nutrient conditions but decompensate when palmitate stress is applied. Chronic palmitate treatment is known to promote mitochondrial cytochrome c release in beta-cells (Maedler et al., 2001; Molina et al., 2009). The inability to maintain intact cristae structures under nutrient stress conditions in SLC25A46 mutant beta-cells may favor cytochrome c release in palmitate-induced apoptosis. Our findings show that although there are compensatory mechanisms preventing the induction of apoptosis, absence of this protein on the outer mitochondrial membrane dramatically sensitizes insulin secreting cells to nutrient stress.

In summary, we identified SLC25A46 as a novel downstream effector of glucose-induced calcium signaling in pancreatic beta-cells. This protein plays a central role in the control of mitochondrial fission. However, the molecular function of SLC25A46 is not likely limited to the regulation of mitochondrial dynamics. Earlier work strongly suggests its involvement in basic mitochondrial processes such as cristae morphology and respiratory activity. SLC25A46 mutant insulin secreting cells are unremarkable in this respect as they respire normally and are able to perform all aspects of

metabolism secretion coupling, which are known to depend on mitochondrial function. Importantly, we observe that insulin secreting cells lacking SLC25A46 are strongly sensitized to palmitate-induced apoptosis. The possible involvement of SLC25A46 in the regulation of mitochondria and the control of apoptosis is an important topic for future research.

Material and Methods

Reagents

Oligomycin (75351), Rotenone (R8875), Antimycin (A8674), FCCP (C2920) Hepes (H3375), EGTA (E3889), Tris (T1503), Glycine (G8898), MDA (M-012), TBA (T5500), Sucrose (S0389), HCl (H1758), SDS (L3771), MgSO4 (M7506), NaCl (S9888), CaCl2 (C1016), KCl (P3911), NaH2PO4 (S0751), Palmitic acid (P5585), Bovine Serum Albumin (A8806), FK506 (F4679) and Cyclosporin A (30024) were acquired from Sigma-Aldrich (St. Louis, MO, USA). Lipofectamine 2000 (10696153) and BCA Protein Assay Kit (10678484) were acquired form Thermo Fisher Scientific (Waltham, MA, USA). AICAR (2840) and carbachol (2810) were acquired from Tocris Bioscience (Bristol, UK). 911 (S8654) was acquired from Selleckchem (Huston, USA). SLC25A46-Myc-DDK (RR209520: Origene), SLC25A46-tGFP (MG206612) and COX8(MTS)-RFP expressing plasmids (RC100126) were acquired from Origene (USA). The YC3.6cyto (fluorescent protein yellow cameleon version 3.6) pcDNA3 construct was kindly provided by Prof. A. Miyawaki (Riken Brain Science Institute, Wako, Japan). Other reagents and provider are indicated in the respective method section.

INS-1E cell culture

INS-1E cells were cultured at 37 °C in a humidified atmosphere (5% CO_2) in RPMI-1640 medium (Thermo) that contained 11 mM glucose, supplemented with 10 mM HEPES (pH 7.3), 10% (v/v) heat-inactivated fetal calf serum (Chemie Brunschwig, Switzerland), 1 mM sodium pyruvate, 50 µM 2-ME, 50 µg/ml penicillin, and 100 µg/ml streptomycin. INS-1E cells were obtained from Pierre Maechler laboratory at the University of Geneva and they were recently authenticated and tested for contamination.

Phosphoproteomic data re-analysis

Our recent study describing the phosphoproteome dynamics over the first hour of glucose stimulation in insulin secreting cells (Santo-Domingo et al., 2019) was reanalyzed in the current work with the aim to increase the chances to capture new glucose-regulated mitochondrial phosphoproteins. Scaffold PTM (Proteome Software, Portland, OR, USA) parameters were here modified to keep all phosphorylated peptides whatever was the modification localization probability (*i.e.*, minimum localization probability was set to 0%). Of note, peptide SFGSGTELGHWVTTPPDIPGSR of SLC25A46 was confidently identified as di-phosphorylated but previously unreported because its phosphorylation sites were assigned with only 40% probability to S35 and T45. The newly generated protein list of glucose-regulated phosphorylated sites (p-value < 0.05) was analyzed in Mitominer 4.0 (http://mitominer.mrc-mbu.cam.ac.uk/release-4.0/begin.do) using the IMPI database (rat mitochondrial proteome) as reference to obtain evidence of mitochondrial localization.

Western blots

For glucose-stimulated experiments 60 mm diameter petri dishes were seeded with 2×10^6 INS-1E cells, and maintained in the incubator for 48 h until they reached 70–80% confluence. The day of the experiment, INS-1E cells were equilibrated in KRBH containing 2.5 mM glucose for 30 min at 37 °C. Subsequently, the plates were divided in two experimental groups and incubated either with 16.7 mM (high glucose) or maintained in 2.5 mM glucose in the same KRBH (low glucose). Cell lysis was carried out after 60min of stimulation or at the time points indicated in the figures. Cells were lysed for 15 min on ice in RIPA buffer that was supplemented with protease inhibitors (Roche, Basel, Switzerland), phosSTOP phosphatase inhibitor cocktail (Roche), 10 mM NaF, 0.1 µM PMSF, and 2 mM Na-orthovanadate for complete phosphatase inhibition. Lysate was centrifuged at 14,000 *g* for 20 min at 4 °C, and the protein content of the supernatant was determined by using Pierce BCA Protein Assay Kit (Pierce, USA). An amount of 25 µg of total protein was loaded onto SDS-PAGE gels. For immunoblotting, proteins were transferred onto nitrocellulose membrane with i-blot (Thermo Fisher Scientific) and probed with the following antibodies: anti-SLC25A46 (12277-1-AP; Protein Tech), anti-DDK (TA50011-100; Origene), anti-AMPKα (#2532; Cell Signaling), anti-AMPKα-pThr172 (#2535; Cell Signaling) 1/1000, anti-tubulin (05-829; Chemicon, Temecula, CA, USA), Anti-Drp1 (YZ6211, YenZyme Antibodies), anti-Drp1 p-637 (YZ5447, YenZyme Antibodies), anti-Opa1 (612606; BD Biosciences), anti-Mfn1 (YZ5443; YenZyme Antibodies), anti-Mfn2 (YZ5445; YenZyme Antibodies), anti-Tom20 (Santa Cruz Biotechnology, Dallas, TX, USA), anti-PanCaderin (#4068; Cell Signaling), anti-GAPDH (ab8245; Abcam), anti-turboGFP (TA150041; Origene). All antibodies were used at 1/1000 dilution. Horseradish peroxidase–conjugated secondary antibodies were used, followed by chemiluminescence detection (Amersham Biosciences, Pittsburgh, PA, USA).

Phospho-specific antibodies anti-Thr44 SLC25A46 and anti-Thr44/45 SLC25A46 were produced by YenZyme Antibodies (Brisbane, CA, USA). Briefly, modified (phosphorylated) peptides were synthetized. The phosphorylated peptides were conjugated to a carrier protein to render then immunogenic and two rabbits were immunized. For each antibody, the elicited antibody was affinity-purified against the same modified peptide used for immunization. Finally, purified antibody was affinity absorbed against the non-modified peptide counterpart to separate the phospho-specific antibody from the cross-reactive antibody populations. For lambda phosphatase assays, cell lysates were either mock or lambda phosphatase (P0753, New England Biolabs) treated for 60 minutes at 30°C with 400U.

INS-1E adenovirus infection

Adenoviral production was performed by Sirion Biotech (Germany). Briefly, SLC25A46-DDK and luciferase ORFs were cloned into pO6A5-CMV adenoviral shuttle vectors. CAP packaging cells were transfected and subsequently lysed to recover SLC25A46-DDK and luciferase infection particles. For the experiments, INS1E cells were infected 2 days after plating. To achieve SLC25A46 overexpression samples were infected with 20 infection units/cell of SLC25A46-DDK adenovirus particles for 90 min in RPMI medium at 37°C. Experimental controls were infected with 20 infection units/cell of luciferase adenovirus particles. Cells were washed with phosphate-buffered saline buffer (PBS) before adding fresh INS-1E cell culture medium. The measurements were performed 24 h after infection.

Mutagenesis and cloning

SLC25A46 T44/45A phospho null mutant was generated by site-directed mutagenesis using the kit GeneArt ® Site-Directed Mutagenesis PLUS (Invitrogene). The following set of oligonucleotides were used to introduce the nucleotide changes:

FW: CTGGGCCACTGGGTGGCAGCACCCCCGGACATCC.

RV: GGATGTCCGGGGGTGCTGCCACCCAGTGGCCCAG.

SLC25A46-wt and SLC25A46 T44/45A doxycycline-induced plasmids were generated by cloning the corresponding full cDNA sequences of both versions of the gene on Tet-On® 3G Inducible Expression System (631168, Takara).

Oxygen consumption

Oxygen consumption in INS-1E cells was measured by using an XF96 instrument (Seahorse Bioscience, Billerica, MA, USA). INS-1E cells were seeded onto polyornithine-coated tissue culture plates (Seahorse Biosciences) at a density of 20,000 cells per well. Two days later, INS-1E were washed twice and incubated in basal Krebs-Ringer bicarbonate HEPES (KRBH) buffer that contained 2.5 mM glucose, 140 mM NaCl, 3.6 mM KCl, 0.5 mM NaH_2PO_4,0.5 mM $MgSO_4$,1.5 mM $CaCl_2$, 10 mM HEPES, and 5 mM $NaHCO_3$ (pH 7.4). Respiration rates were determined every 6 min. All experiments were performed at 37 °C. Respiratory chain inhibitors were added as indicated in the figures at the following concentrations: rotenone, 1 µM; antimycin A, 1 µg/ml; oligomycin, 2,5 µg/ml.

Calcium imaging

Cytosolic Ca^{2+} was measured with the genetically encoded sensor YC3.6cyto or Fura2. For calcium measurements based on YC3.6cyto, INS-1E cells were plated on polyornithin-treated glassbottom dishes (35 mm diameter; MatTek, Ashland, MA, USA) and transfected with pcDNA3 YC3.6cyto using Jetprime transfection reagent (Polyplus-Transfection SA, Illkirch-Graffenstaden, France). Two days after transfection, cells were imaged on KRBH buffer. For Fura 2 measurements, cells were incubated 40 min in KRBH buffer containing 2 µM Fura2-AM at room temperature, followed by 30 min in KRBH. Cells were imaged on KRBH. Glass coverslips were inserted in a thermostatic chamber (Life Imaging Services, Basel, Switzerland) that was maintained at 37 °C. Cells were imaged on a DMI6000 B inverted fluorescence microscope using an HCX PL APO ×63>/1.40–0.60 NA oil immersion objective (Leica Microsystems, Wetzlar, Germany) and an Evolve 512 back-illuminated charge-coupled device with 16×16-pixel camera (Photometrics, Tucson, AZ, USA). For YC3.6cyto measurements, cells were excited at 430 nm through a BP436/20 filter. Two emission images were acquired with BP480/40 and BP535/30 emission filters. For Fura2 measurements, cells were alternatively exited with the BP340/10 and BP387/10 filters and emission was collected with BP535/25 filter. Background was subtracted, fluorescence ratios were calculated in MetaFluor 7.0 (Meta Imaging Series; Molecular Devices, Sunnyvale, CA, USA) and analyzed in Excel (Microsoft, Redmond, WA, USA) and GraphPad Prism 5 (GraphPad Software, La Jolla, CA, USA). Images were taken every 2 s.

Static insulin secretion

INS-1E cells were plated on a polyornithine-treated 24-well plate. After 48 h, cells were washed in Krebs-Ringer bicarbonate HEPES buffer (KRBH), containing (in mM): 140 NaCl, 3.6 KCl, 0.5

NaH_2PO_4, 0.5 $MgSO_4$, 1.5 $CaCl_2$, 10 HEPES, 5 $NaHCO_3$, and pH 7.4 with 2.5 mM glucose. Cells were stimulated for 30 min with 16.7 mM glucose and supernatants were collected. Cellular insulin content was extracted with a mixture of ethanol (75%) and HCl (1.5%) overnight at 4 °C. Insulin was measured using a Rat Insulin Enzyme Immunoassay Kit (SpiBio, Montigny-le-Bretonneux, France).

INS-1E SLC25A46 KO generation

sgRNA was designed using CHOPCHOP (https://chopchop.rc.fas.harvard.edu/) and cloned into Cas9-sgRNA lentiviral vector (pLenti-U6-sgRNA-SFFV-Cas9-2A-Puro; abm®). The target sequence was GCGGACGGCACACCGTACGA (Rattus norvegicus, NM_001100515). Lentivirus production was performed according to abm protocol as described on the website (https://www.abmgood.com/Lentivirus-Packaging-Systems.html). For transduction, a MOI of 5 was used to transduce 2×10^5 wild type INS-1E cells. Puromycin selection was performed two days after transduction using 1.1 µg/ml of G264. After puromycin selection, genomic DNA was extracted for PCR. The PCR product was sequenced and compared to the reference genome. Following puromycin selection, the polyclonal pools with indels that induce frame shift mutations were selected for further expansion. Subsequently, monoclonal selection was performed *via* single cell dilution and cell underwent drug selection at the same time. Clones were then screened using CRISPR Genomic Cleavage Detection Kit (G932, abm) and successful clones were further submitted to Sanger Sequencing validation (forward primer sequence: 5' – GCTACGGAGAAGTCACCCAG - 3' and reverse primer sequence: 5' – GTGACTCCACCTATAGGCGC - 3'). Sequencing results showing frame shift mutations confirmed successful genome editing (Suppl. Fig.2).

Transmission electron microscopy (sample preparation)

INS-1E cells were seeded, allowed to attach on polyornithine coated coverslips (Nalge Nunc Int. #174969) and cultured for 4 days. The cells were then washed twice briefly with PBS pH 7.4 and fixed for 1 hour in PBS containing 2% paraformaldehyde and 2.5% glutamine at room temperature. The cells were washed 3 times at 4 °C in cacodylate buffer (0.1 M, pH 7.4). The samples were postfixed twice for 40 minutes at room temperature in cacodylate buffer (0.1 M, pH 7.4) with 1% osmium tetroxide. The cells were washed for 5 minutes in distilled water and stained for 40 minutes in 1 % uranyl acetate. The cells were washed for an additional 5 minutes in distilled water and dehydrated in a graded alcohol series (1× 50 %, 1× 70 %, 2x 96 %, 2× 100 %). The cells were embedded in Durcupan. The samples were placed on coated glass slides and left overnight at 65 °C.

Mitochondrial isolation

Approximately 80% confluent INS-1E cells from two 75-cm^2 flasks were washed with PBS and detached by trypsinization. The cell suspension was centrifuged at room temperature (1000rpm, 5min). The cell pellet was resuspended in 1ml of sucrose/TES buffer (300 mM sucrose, 10 mM TES, 0.5 mM EGTA, pH 7.4) and incubated for 1 h on ice. Subsequently, the cells were lysed in a glass homogenizer and centrifuged at 4 °C (200 *g* for 10 min). The mitochondria-containing supernatant was subjected to a second centrifugation at 4ºC (6,000 *g* for 15min). Finally, the mitochondrial containing pellet was resuspended in 100µl of RIPA buffer for Western analysis.

Mitochondrial network connectivity

Fluorescence recovery after photobleaching (FRAP) was used to measure mitochondrial connectivity. INS-1E cells were plated on polyornithin-treated glassbottom dishes (35 mm diameter; MatTek, Ashland, MA, USA) and transfected with mitochondrial matrix-targeted RFP (Cox8-RFP, Origene, USA) using Jetprime transfection reagent (Polyplus-Transfection SA, Illkirch-Graffenstaden, France). Two days after transfection cells were imaged at 37 °C on a SP5 confocal microscope (Leica Microsystems, Wetzlar, Germany). Experiments and image analysis were performed using the LAS AF FRAP wizard (Leica Microsystems, Wetzlar, Germany). Mitochondrial network was imaged on the confocal microscope SP5 using a X63 objective. Samples were excited with the 561 nm laser line and emission was collected between 570-700 nm. Five images were acquired (3 images/second) before applying one single bleaching pulse (100 ms, 571 nm laser, 70% power, 7.0 width × 2.0 height µm areas) followed by live imaging initially at 1 frame/second for 1 min and later at 0.2 frame/second for an additional minute to allow RFP equilibration across the lumen of the mitochondrial network. Loss of focus and movement artifacts were minimized by using a large pinhole aperture (2.00 AU). “Zoom in” and “Set background to zero” modes were respectively set to reduce the scan field during photobleaching and to prevent that the background outside the exposed ROI is bleached.

Representative images of mitochondrial networks were also obtained by confocal imaging. Briefly, Confocal Z-stacks of cells expressing the matrix-targeted red fluorescent protein Cox8(MTS)-RFP were acquired on a SP5 confocal microscope (Leica Microsystems, Wetzlar, Germany) inverted Microscope using a X63 objective, 561 nm excitation and 570-700 nm emission. 15 z-stack images per cell were projected using the Image J tool ‘Z-projection’ to generate complete mitochondrial network images. Images of single cell mitochondrial networks were qualitatively classified in blind scrutiny as fragmented, intermediate and hyperfused (300 cells per condition; three experiments).

Apoptosis assay

Annexin V-labelled apoptotic cells were imaged with the Incucyte ZOOM live cell analysis system (Essen bioscience). INS-1E cells were plated at 40000 cells/well in 96-well plates, 24 h prior to the experiments. For the assay, FITC-labelled Annexin V (Incucyte® Annexin V Green) and treatments (BSA-Palmitate and BSA) were added to the complete INS-1E growth medium according to the manufacturer's instructions (Incucyte Zoom, Sartorious). Cells were incubated at 37 °C and 5% CO_2 in the presence of fluorescently labelled Annexin V. Images were taken with 10× objective every 4 hours (Excitation: 460 nm; Passband: [440,480] nm Emission: 524 nm; Passband: [504,544]) and processed with the Incucyte Zoom software. Briefly, a training set of images including untreated and staurosporine-induced apoptosis cells was analyzed with the Incucyte ZOOM image analysis tool to establish a set of internal parameters for an image processing definition that optimally separate positive cells from background. Settings for segmentation were as follows: “Adaptive Background”, Threshold (GCU) “2.000”, Edge Split “of”, Edge Sensitivity “off”; Cleanup: Hole Fill (μm^2) “off” and Filters for Area, Eccentricity, mean intensity and integrated intensity “off”. This set of internal parameters were subsequently applied to the whole image collection. Images were segmented and apoptosis was quantified as total integrated apoptotic intensity (GCU × μm^2 / image).

Lipid peroxidation

Quantification of lipid peroxidation was carried out using the TBARS assay. Approximately 80% confluent INS-1E cells from 60 mm-diameter culture plates were washed with phosphate-buffered saline buffer (PBS) and detached by trypsinization. Then, cell suspensions were centrifuge at 200-300 g for 4 minutes and the pellets frozen at -80ºC. After 1 hour cell pellets were thawed at room temperature, resuspended in 15µl PBS and vigorously homogenized to achieve mechanical rupture of the cells. At this point, 12 µl of the suspension was collected in a new Eppendorf for the TBARS assay (the remaining volume was transferred for BCA assay). Samples were subsequently treated with 390 µl of 0,2M Glycine-HCl pH 3,6 buffer and 250 µl of a 0,5%TBA - 2%SDS solution and incubated at 90ºC for 45 minutes in the absence of light. For measurements, 200ul of each sample was transferred to a 96 well-plate and read at 523 nm in a SpectraMax® ABS Plus spectrophotometer (Molecular Devices)**.** Finally, optical density values were interpolated against a 0 to 80 µM MDA calibration curve to obtain lipid peroxides concentrations as µM MDA and normalized by protein content.

Statistical analysis

All statistical analyses were performed using Prism software (GraphPad). Significance between two experimental groups was determined using a Student's *t*-test whereas group sets were analyzed using ANOVA (post-hoc test used Tukey). NS: Non-significant; *: p-value < 0,05; **: p-value < 0,01; ***: p-value < 0,001.

Competing interest

Steve Lassueur, Antonio Núñez Galindo, Loïc Dayon and Andreas Wiederkehr were employed by Société des Produits Nestlé S.A. during the generation of this manuscript.

Funding

This study was founded by Nestle Research (Switzerland) and Programa Estratégico Instituto de Biología y Genética Molecular (IBGM) de Valladolid. Ref. CCVC8485 (Spain). The study sponsor was not involved in the design of the study, the collection, analysis and interpretation of data, or writing the report, and did not impose any restrictions regarding the publication of the report.

Acknowledgments

The authors thank Jorge Mondejar-Durán for the technical advice and discussions with TBARS experiments. A especial thanks to Proyecto de Internacionalización de la Unidad de Excelencia Instituto de Biología y Genética Molecular (IBGM) de Valladolid, Ref. CL-EI-2021 IBGM (Spain), and Programa Estratégico Instituto de Biología y Genética Molecular (IBGM) de Valladolid. Ref. CCVC8485 (Spain) for the financial support provided.

References

Abrams, A. J., Hufnagel, R. B., Rebelo, A., Zanna, C., Patel, N., Gonzalez, M. A., Campeanu, I. J., Griffin, L. B., Groenewald, S., Strickland, A. v., Tao, F., Speziani, F., Abreu, L., Schüle, R., Caporali, L., la Morgia, C., Maresca, A., Liguori, R., Lodi, R., … Dallman, J. E. (2015). Mutations in SLC25A46, encoding a UGO1-like protein, cause an optic atrophy spectrum disorder. *Nature Genetics*, *47*(8), 926–932. https://doi.org/10.1038/NG.3354.

Antinozzi, P.A., Ishihara, H., Newgard, C. B., Wollheim, C. B. Mitochondrial metabolism sets the maximal limit of fuel-stimulated insulin secretion in a model pancreatic beta cell: a survey of four fuel secretagogues. (2002) *Journal of Biological Chemistry*, *277*(14), 11746-55. http://doi.org/10.1074/JBC.M108462200.

de Marchi, U., Thevenet, J., Hermant, A., Dioum, E., & Wiederkehr, A. (2014). Calcium co-regulates oxidative metabolism and ATP synthase-dependent respiration in pancreatic beta cells. *The Journal of Biological Chemistry*, *289*(13), 9182–9194. https://doi.org/10.1074/JBC.M113.513184

de Vos, A., Heimberg, H., Quartier, E., Huypens, P., Bouwens, L., Pipeleers, D., & Schuit, F. (1995). Human and rat beta cells differ in glucose transporter but not in glucokinase gene expression. *The Journal of Clinical Investigation*, *96*(5), 2489–2495. https://doi.org/10.1172/JCI118308

Eizirik, D. L., Korbutt, G. S., & Hellerström, C. (1992). Prolonged exposure of human pancreatic islets to high glucose concentrations in vitro impairs the beta-cell function. *The Journal of Clinical Investigation*, *90*(4), 1263–1268. https://doi.org/10.1172/JCI115989

El-Assaad, W., Buteau, J., Peyot, M. L., Nolan, C., Roduit, R., Hardy, S., Joly, E., Dbaibo, G., Rosenberg, L., & Prentki, M. (2003). Saturated fatty acids synergize with elevated glucose to cause pancreatic beta-cell death. *Endocrinology*, *144*(9), 4154–4163. https://doi.org/10.1210/EN.2003-0410

Frezza, C., Cipolat, S., Martins de Brito, O., Micaroni, M., Beznoussenko, G. v., Rudka, T., Bartoli, D., Polishuck, R. S., Danial, N. N., de Strooper, B., & Scorrano, L. (2006). OPA1 controls apoptotic cristae remodeling independently from mitochondrial fusion. *Cell*, *126*(1), 177–189. https://doi.org/10.1016/J.CELL.2006.06.025

Germain, M., Mathai, J. P., McBride, H. M., & Shore, G. C. (2005). Endoplasmic reticulum BIK initiates DRP1-regulated remodelling of mitochondrial cristae during apoptosis. *The EMBO Journal*, *24*(8), 1546–1556. https://doi.org/10.1038/SJ.EMBOJ.7600592

Griesche, N., Sanchez, G., Hermans, C., & Idevall-Hagren, O. (2019). Cortical mitochondria regulate insulin secretion by local Ca 2+ buffering in rodent beta cells. *Journal of Cell Science*, *132*(9). https://doi.org/10.1242/JCS.228544

Heit, J. J., Apelqvist, Å. A., Gu, X., Winslow, M. M., Neilson, J. R., Crabtree, G. R., & Kim, S. K. (2006). Calcineurin/NFAT signalling regulates pancreatic beta-cell growth and function. *Nature*, *443*(7109), 345–349. https://doi.org/10.1038/NATURE05097

Hellman, B., Idahl, L. A., Lernmark, A., Sehlin, J., & Täljedal, I. B. (1974). The pancreatic beta-cell recognition of insulin secretagogues. Effects of calcium and sodium on glucose metabolism and insulin release. *The Biochemical Journal*, *138*(1), 33–45. https://doi.org/10.1042/BJ1380033

Hennings, T. G., Chopra, D. G., DeLeon, E. R., VanDeusen, H. R., Sesaki, H., Merrins, M. J., & Ku, G. M. (2018). In Vivo Deletion of β-Cell Drp1 Impairs Insulin Secretion Without Affecting Islet Oxygen Consumption. *Endocrinology*, *159*(9), 3245–3256. https://doi.org/10.1210/EN.2018-00445

Janer, A., Prudent, J., Paupe, V., Fahiminiya, S., Majewski, J., Sgarioto, N., des Rosiers, C., Forest, A., Lin, Z., Gingras, A., Mitchell, G., McBride, H. M., & Shoubridge, E. A. (2016). SLC25A46 is required for mitochondrial lipid homeostasis and cristae maintenance and is responsible for Leigh syndrome. *EMBO Molecular Medicine*, *8*(9), 1019–1038. https://doi.org/10.15252/EMMM.201506159

Jansson, D., Ng, A. C. H., Fu, A., Depatie, C., al Azzabi, M., & Screaton, R. A. (2008). Glucose controls CREB activity in islet cells via regulated phosphorylation of TORC2. *Proceedings of the National Academy of Sciences of the United States of America*, *105*(29), 10161–10166. https://doi.org/10.1073/PNAS.0800796105

Jhun, B. S., Lee, H., Jin, Z. G., & Yoon, Y. (2013). Glucose stimulation induces dynamic change of mitochondrial morphology to promote insulin secretion in the insulinoma cell line INS-1E. *PloS One*, *8*(4). https://doi.org/10.1371/JOURNAL.PONE.0060810

Kabra, U. D., Pfuhlmann, K., Migliorini, A., Keipert, S., Lamp, D., Korsgren, O., Gegg, M., Woods, S. C., Pfluger, P. T., Lickert, H., Affourtit, C., Tschöp, M. H., & Jastroch, M. (2017). Direct Substrate Delivery Into Mitochondrial Fission-Deficient Pancreatic Islets Rescues Insulin Secretion. *Diabetes*, *66*(5), 1247–1257. https://doi.org/10.2337/DB16-1088

Kozjak-Pavlovic, V. (2017). The MICOS complex of human mitochondria. *Cell and Tissue Research*, *367*(1), 83–93. https://doi.org/10.1007/S00441-016-2433-7

Lee, Y. J., Jeong, S. Y., Karbowski, M., Smith, C. L., & Youle, R. J. (2004). Roles of the mammalian mitochondrial fission and fusion mediators Fis1, Drp1, and Opa1 in apoptosis. *Molecular Biology of the Cell*, *15*(11), 5001–5011. https://doi.org/10.1091/MBC.E04-04-0294

Liesa, M., Palacín, M., & Zorzano, A. (2009). Mitochondrial dynamics in mammalian health and disease. *Physiological Reviews*, *89*(3), 799–845. https://doi.org/10.1152/PHYSREV.00030.2008

Maedler, K., Spinas, G. A., Dyntar, D., Moritz, W., Kaiser, N., & Donath, M. Y. (2001). Distinct effects of saturated and monounsaturated fatty acids on beta-cell turnover and function. *Diabetes*, *50*(1), 69–76. https://doi.org/10.2337/DIABETES.50.1.69

Molina, A. J. A., Wikstrom, J. D., Stiles, L., Las, G., Mohamed, H., Elorza, A., Walzer, G., Twig, G., Katz, S., Corkey, B. E., & Shirihai, O. S. (2009). Mitochondrial networking protects beta-cells from nutrient-induced apoptosis. *Diabetes*, *58*(10), 2303–2315. https://doi.org/10.2337/DB07-1781

Nakano, K., Yanobu-Takanashi, R., Shimizu, Y., Takahashi, Y., Hiura, K., Watanabe, M., Sasaki, H., Okamura, T., & Sasaki, N. (2020). Genetic locus responsible for diabetic phenotype in the insulin hyposecretion (ihs) mouse. *PloS One*, *15*(6). https://doi.org/10.1371/JOURNAL.PONE.0234132

Neupert, W. (2012). SnapShot: Mitochondrial architecture. *Cell*, *149*(3), 722-722.e1. https://doi.org/10.1016/J.CELL.2012.04.010

Olichon, A., Baricault, L., Gas, N., Guillou, E., Valette, A., Belenguer, P., & Lenaers, G. (2003). Loss of OPA1 perturbates the mitochondrial inner membrane structure and integrity, leading to cytochrome c release and apoptosis. *The Journal of Biological Chemistry*, *278*(10), 7743–7746. https://doi.org/10.1074/JBC.C200677200

Palmieri, F. (2013). The mitochondrial transporter family SLC25: identification, properties and physiopathology. *Molecular Aspects of Medicine*, *34*(2–3), 465–484. https://doi.org/10.1016/J.MAM.2012.05.005

Park, K. S., Wiederkehr, A., Kirkpatrick, C., Mattenberger, Y., Martinou, J. C., Marchetti, P., Demaurex, N., & Wollheim, C. B. (2008). Selective actions of mitochondrial fission/fusion genes on metabolism-secretion coupling in insulin-releasing cells. *The Journal of Biological Chemistry*, *283*(48), 33347–33356. https://doi.org/10.1074/JBC.M806251200

Pich, S., Bach, D., Briones, P., Liesa, M., Camps, M., Testar, X., Palacín, M., & Zorzano, A. (2005). The Charcot-Marie-Tooth type 2A gene product, Mfn2, up-regulates fuel oxidation through expression of OXPHOS system. *Human Molecular Genetics*, *14*(11), 1405–1415. https://doi.org/10.1093/HMG/DDI149

Reinhardt, F., Schultz, J., Waterstradt, R., & Baltrusch, S. (2016). Drp1 guarding of the mitochondrial network is important for glucose-stimulated insulin secretion in pancreatic beta cells. *Biochemical and Biophysical Research Communications*, *474*(4), 646–651. https://doi.org/10.1016/J.BBRC.2016.04.142

Rorsman, P., & Ashcroft, F. M. (2018). Pancreatic β-Cell Electrical Activity and Insulin Secretion: Of Mice and Men. *Physiological Reviews*, *98*(1), 117–214. https://doi.org/10.1152/PHYSREV.00008.2017

Ruprecht, J. J., & Kunji, E. R. S. (2020). The SLC25 Mitochondrial Carrier Family: Structure and Mechanism. *Trends in Biochemical Sciences*, *45*(3), 244–258. https://doi.org/10.1016/J.TIBS.2019.11.001

Santo-Domingo, J., Galindo, A. N., Cominetti, O., de Marchi, U., Cutillas, P., Dayon, L., & Wiederkehr, A. (2019). Glucose-dependent phosphorylation signaling pathways and crosstalk to mitochondrial respiration in insulin secreting cells. *Cell Communication and Signaling : CCS*, *17*(1). https://doi.org/10.1186/S12964-019-0326-6

Schuit, F., de Vos, A., Farfari, S., Moens, K., Pipeleers, D., Brun, T., & Prentki, M. (1997). Metabolic fate of glucose in purified islet cells. Glucose-regulated anaplerosis in beta cells. *The Journal of Biological Chemistry*, *272*(30), 18572–18579. https://doi.org/10.1074/JBC.272.30.18572

Screaton, R. A., Conkright, M. D., Katoh, Y., Best, J. L., Canettieri, G., Jeffries, S., Guzman, E., Niessen, S., Yates, J. R., Takemori, H., Okamoto, M., & Montminy, M. (2004). The CREB coactivator TORC2 functions as a calcium- and cAMP-sensitive coincidence detector. *Cell*, *119*(1), 61–74. https://doi.org/10.1016/J.CELL.2004.09.015

Sesaki, H., & Jensen, R. E. (2001). UGO1 encodes an outer membrane protein required for mitochondrial fusion. *The Journal of Cell Biology*, *152*(6), 1123–1134. https://doi.org/10.1083/JCB.152.6.1123

Sesaki, H., & Jensen, R. E. (2004). Ugo1p links the Fzo1p and Mgm1p GTPases for mitochondrial fusion. *The Journal of Biological Chemistry*, *279*(27), 28298–28303. https://doi.org/10.1074/JBC.M401363200

Shah, P., Ardestani, A., Dharmadhikari, G., Laue, S., Schumann, D. M., Kerr-Conte, J., Pattou, F., Klein, T., & Maedler, K. (2013). The DPP-4 inhibitor linagliptin restores β-cell function and survival in human isolated islets through GLP-1 stabilization. *The Journal of Clinical Endocrinology and Metabolism*, *98*(7). https://doi.org/10.1210/JC.2013-1029

Steffen, J., Vashisht, A. A., Wan, J., Jen, J. C., Claypool, S. M., Wohlschlegel, J. A., & Koehler, C. M. (2017). Rapid degradation of mutant SLC25A46 by the ubiquitin-proteasome system results in MFN1/2-mediated hyperfusion of mitochondria. *Molecular Biology of the Cell*, *28*(5), 600–612. https://doi.org/10.1091/MBC.E16-07-0545

Twig, G., Elorza, A., Molina, A. J. A., Mohamed, H., Wikstrom, J. D., Walzer, G., Stiles, L., Haigh, S. E., Katz, S., Las, G., Alroy, J., Wu, M., Py, B. F., Yuan, J., Deeney, J. T., Corkey, B. E., & Shirihai, O. S. (2008). Fission and selective fusion govern mitochondrial segregation and elimination by autophagy. *The EMBO Journal*, *27*(2), 433–446. https://doi.org/10.1038/SJ.EMBOJ.7601963

Wan, J., Steffen, J., Yourshaw, M., Mamsa, H., Andersen, E., Rudnik-Schöneborn, S., Pope, K., Howell, K. B., Mclean, C. A., Kornberg, A. J., Joseph, J., Lockhart, P. J., Zerres, K., Ryan, M. M., Nelson, S. F., Koehler, C. M., & Jen, J. C. (2016). Loss of function of SLC25A46 causes lethal congenital pontocerebellar hypoplasia. *Brain : A Journal of Neurology*, *139*(11), 2877–2890. https://doi.org/10.1093/BRAIN/AWW212

Wiederkehr, A., & Wollheim, C. B. (2012). Mitochondrial signals drive insulin secretion in the pancreatic β-cell. *Molecular and Cellular Endocrinology*, *353*(1–2), 128–137. https://doi.org/10.1016/J.MCE.2011.07.016

Zhang, Z., Wakabayashi, N., Wakabayashi, J., Tamura, Y., Song, W. J., Sereda, S., Clerc, P., Polster, B. M., Aja, S. M., Pletnikov, M. v., Kensler, T. W., Shirihai, O. S., Iijima, M., Hussain, M. A., & Sesaki, H. (2011). The dynamin-related GTPase Opa1 is required for glucose-stimulated ATP production in pancreatic beta cells. *Molecular Biology of the Cell*, *22*(13), 2235–2245. https://doi.org/10.1091/MBC.E10-12-0933

Figures

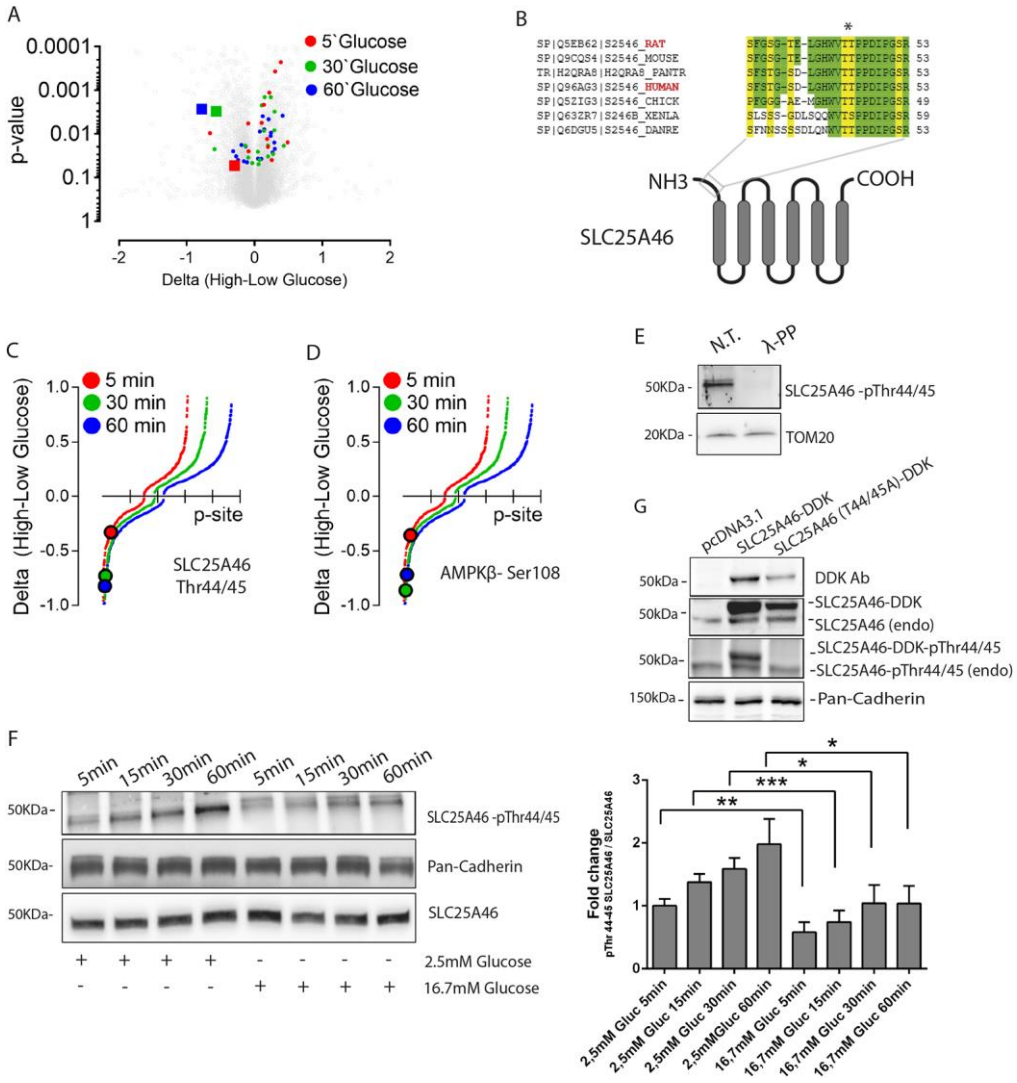

Fig.1. Identification of SLC25A46 as a glucose-regulated mitochondrial phosphoprotein in INS-1E cells. A) Phosphorylation changes of phosphopeptides after stimulation of INS-1E cells with 16.7 mM glucose for 5 min (red), 30 min (green) and 60 min (blue). The values shown were obtained after subtraction of the phospho-peptide abundance in low 2.5 mM glucose. The *p*-values assessing the differences before and after glucose stimulation were obtained from 4 independent experiments. Phosphorylations of the identified SLC25A46 peptide are shown as squares. Results are presented as volcano plots. B) Alignment of the SLC25A46 peptide containing threonines T44 and T45 from different species. The position of this peptide at the N-terminus of the protein, close to the predicted first transmembrane

domain is shown. C and D) Peptides were ranked according to the difference in phosphorylation before and after glucose stimulation for the indicated times. C) SLC25A46-T44/T45 and D) AMPKβ-S108 phosphorylation levels are respectively displayed as larger circles. E) Western blots demonstrating SLC25A46 T44/45 phosphorylation under non stimulatory conditions with an antibody raised against double (pThr44/45) phosphorylated SLC25A46. INS-1E lysates were either non-treated (N.T.) and λ-phosphatase (λ-PP) treated. F) Western blot and graph bar showing the effect of glucose simulation on SLC25A46 T44/45 phosphorylation followed with antibody raised against the double (pThr44/45) phosphorylated SLC25A46 (same antibody as for panel E). INS-1E cells were incubated with two glucose concentrations, respectively, (2.5 and 16.7 mM) for increasing amounts of time as indicated. Graph bar shows average of 6 independent experiments (N=6) +/- SEM. G) Western blots demonstrating the specificity of the antibody recognizing the phosphorylated (pThr44/45) SLC25A46 protein in lysates from control cells, cells transfected with DDK-tagged version of wild type SLC25A46 and cells transfected with a DDK-tagged version encoding a double alanine mutant SLC25A46 A44/A45.

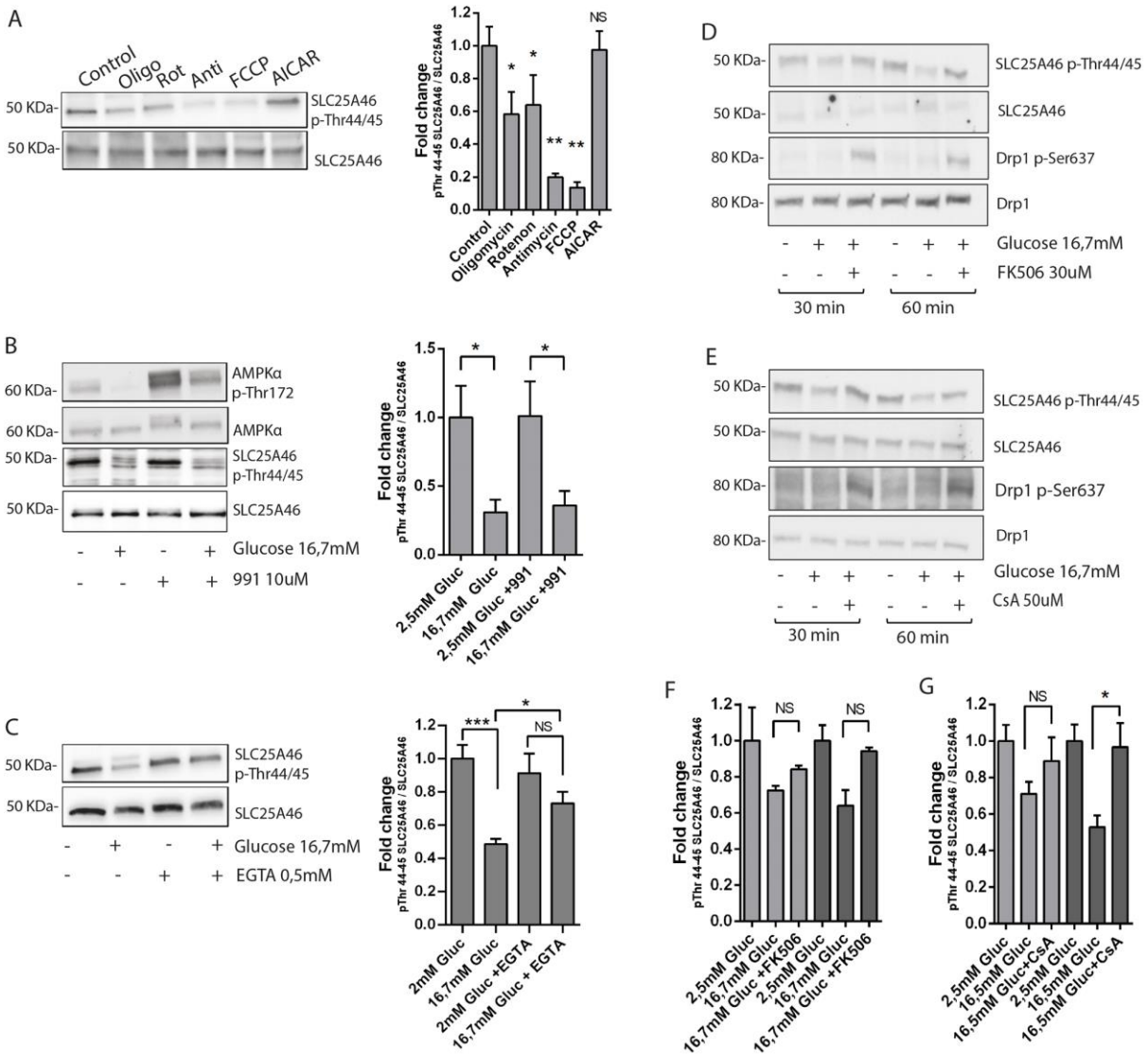

Fig.2. Effect of calcineurin inhibitors on glucose-dependent dephosphorylation of SLC25A46$_{Thr44/45}$. Phosphorylation status of SLC25A46 was assessed with an antibody raised against the peptide phosphorylated on both T44 and T45 (upper blots). For comparison SLC25A46 expression was revealed with an antibody against total SLC25A46 (lower blots). A) Effect of the mitochondrial inhibitors oligomycin (2.5 µg/ml), rotenone (1 µM), antimycin A (1 µg/ml), FCCP (1 µM) and the AMPK activator AICAR (500 µM) on SLC25A46$_{T44/T45}$ phosphorylation. Graph bar shows average of 6 independent experiments (N=6) +/- SEM. B) Effect of glucose stimulation and AMPK activation with 991 (10µM) on AMPK T172 and SLC25A46$_{T44/T45}$ phosphorylation. Cells were exposed to glucose for 60 min. Graph bar shows average of 4 independent experiments (N=4) +/- SEM. C) Glucose-dependent dephosphorylation of SLC25A46$_{T44/T45}$ is blocked after removal of extracellular calcium with

EGTA (0.5 mM). Cells were exposed to glucose for 60 min. Graph bar shows average of 6 independent experiments (N=6) +/- SEM. D) Effect of the calcineurin inhibitor FK506 (30 μM) on SLC25A46$_{T44/T45}$ and Drp1$_{S637}$ phosphorylation in INS-1E cells exposed for 30 and 60 minutes to 16.7 mM glucose (quantification displayed in panel F). E) Effect of the calcineurin inhibitor Cyclosporin A (CsA; 50 μM) on SLC25A46$_{T44/T45}$ and Drp1$_{S637}$ phosphorylation in INS-1E cells exposed for 30 and 60 minutes to 16.7 mM glucose (quantification displayed in panel G). F) Graph bar shows the effect of the calcineurin inhibitor FK506 (30 mM) on SLC25A46$_{T44/T45}$ and Drp1$_{S637}$ phosphorylation in INS-1E cells exposed for 30 (grey bars) and 60 minutes (dark grey bars) to 16.7 mM glucose. Average of 4 independent experiments (N=4) +/- SEM. G) Graph bar shows effect of the calcineurin inhibitor Cyclosporin A (CsA; 50 mM) on SLC25A46$_{T44/T45}$ and Drp1$_{S637}$ phosphorylation in INS-1E cells exposed for 30 (grey bars) and 60 minutes (dark grey bars) to 16.7 mM glucose. Average of 4 independent experiments (N=4) +/- SEM.

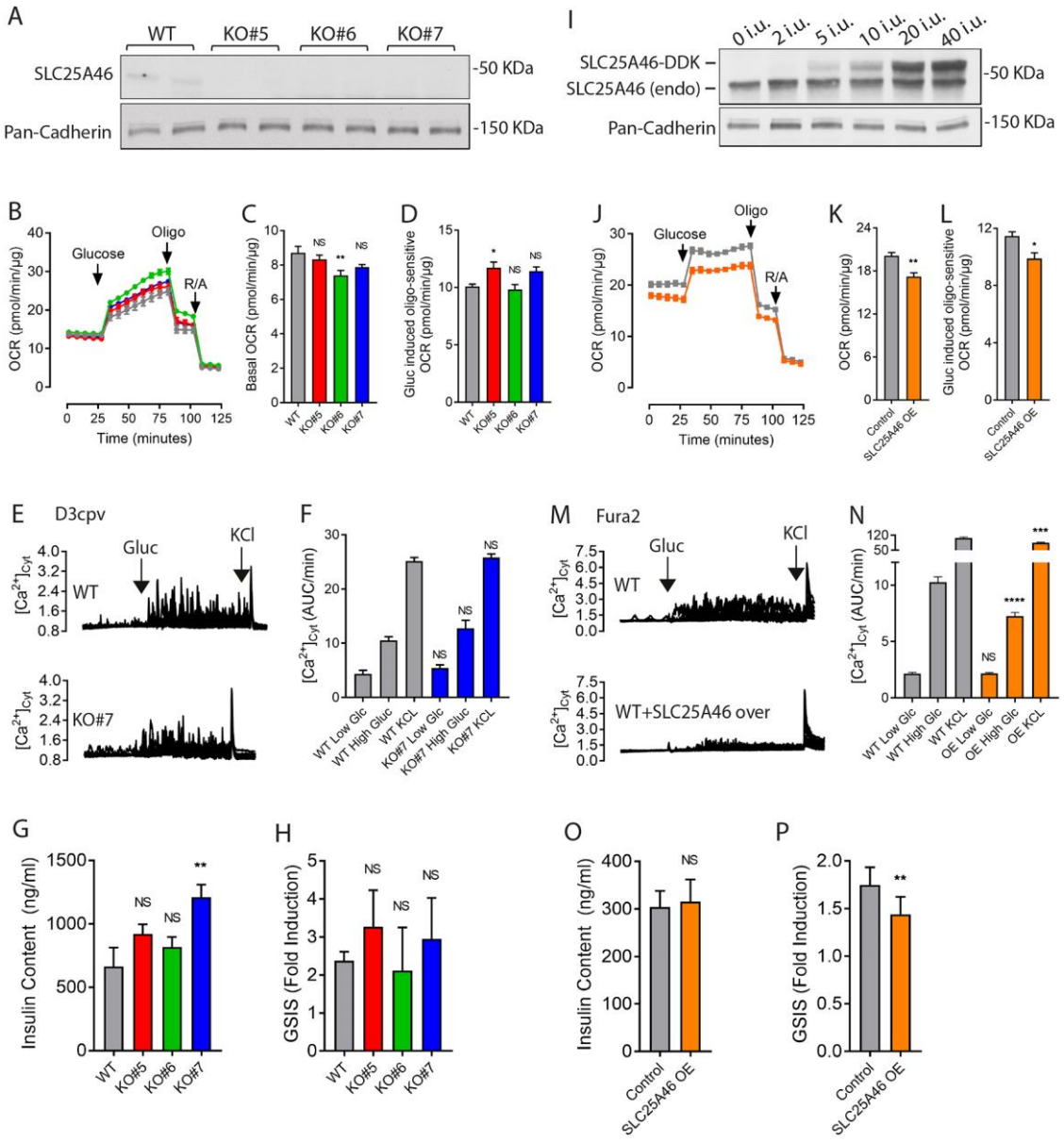

Fig.3. Effect of SLC25A46 protein levels on mitochondrial function and metabolism-secretion coupling in INS-1E cells. A) SLC25A46 protein expression in wild type and three different SLC25A46 deficient INS-1E cell clones (KO#5, KO#6, KO#7) after the gene by Crispr/Cas9. pan-Cadherin detection was used as a loading control. B) Effect of glucose (16.7 mM), oligomycin (conc) and rotenone/antimycin (conc) on oxygen consumption rates in wild type and SLC25A46 deficient clones. C) Effect of SLC25A46 suppression on basal respiration. D) Effect of SLC25A46 suppression on glucose-induced oligomycin dependent oxygen consumption rates. Average of results from 3 independent experiments performed in quadruplicate +/- SEM. E-F) Glucose-induced cytosolic Ca^{2+} signaling measured with the genetically encoded calcium sensor D3cpv. E) Several control INS-1E (upper trace) or

lacking SLC25A46 expression (lower trace) responding to glucose (Gluc 16.7 mM) and KCl (30 mM) are shown. F) Quantification of the area under curve of Ca^{2+} responses in control (grey bars) and SLC25A46 deficient INS-1E cells (blue bars). Average of 3 independent experiments performed in quadruplicate +/- SEM. Total of 30 cells per condition analyzed. G) Effect of SLC25A46 suppression on insulin content. H) Effect of SLC25A46 suppression on the fold induction of insulin secretion when raising glucose from 2.5 to 16.7 mM. Average of 3 independent experiments performed in quadruplicate +/- SEM. I) Western-blot showing endogenous SLC25A46 (lower band) and DDK-SLC25A46 (upper band) expression in INS-1E cells infected with increasing number of particles of adeno-associated virus for the overexpression of DDK-SLC265A46 (u.i. refers to infection units/cell). J) Effect of glucose (16.7 mM), oligomycin (conc) and rotenone/antimycin (conc) on oxygen consumption rate in wild type and SLC25A46 overexpressing cells. K, L) Effect of SLC25A46 overexpression on basal respiration (K), and on glucose-induced oligomycin sensitive respiration (L). Average of results from 3 independent experiments performed in quadruplicate +/- SEM. M, N) Effect of SLC25A46 overexpression on glucose-induced cytosolic Ca^{2+} signaling measured with Fura-2. Quantification of area under the curve of Ca^{2+} signals in response to glucose (16.7 mM) and KCl (30mM) in control (grey bars) and DDK-SLC25A46 transgene expressing cells. O, P) Effect of SLC25A46 overexpression on insulin content (O) and fold glucose-induced insulin secretion (P). Average of 3 independent experiments performed in quadruplicate +/- SEM.

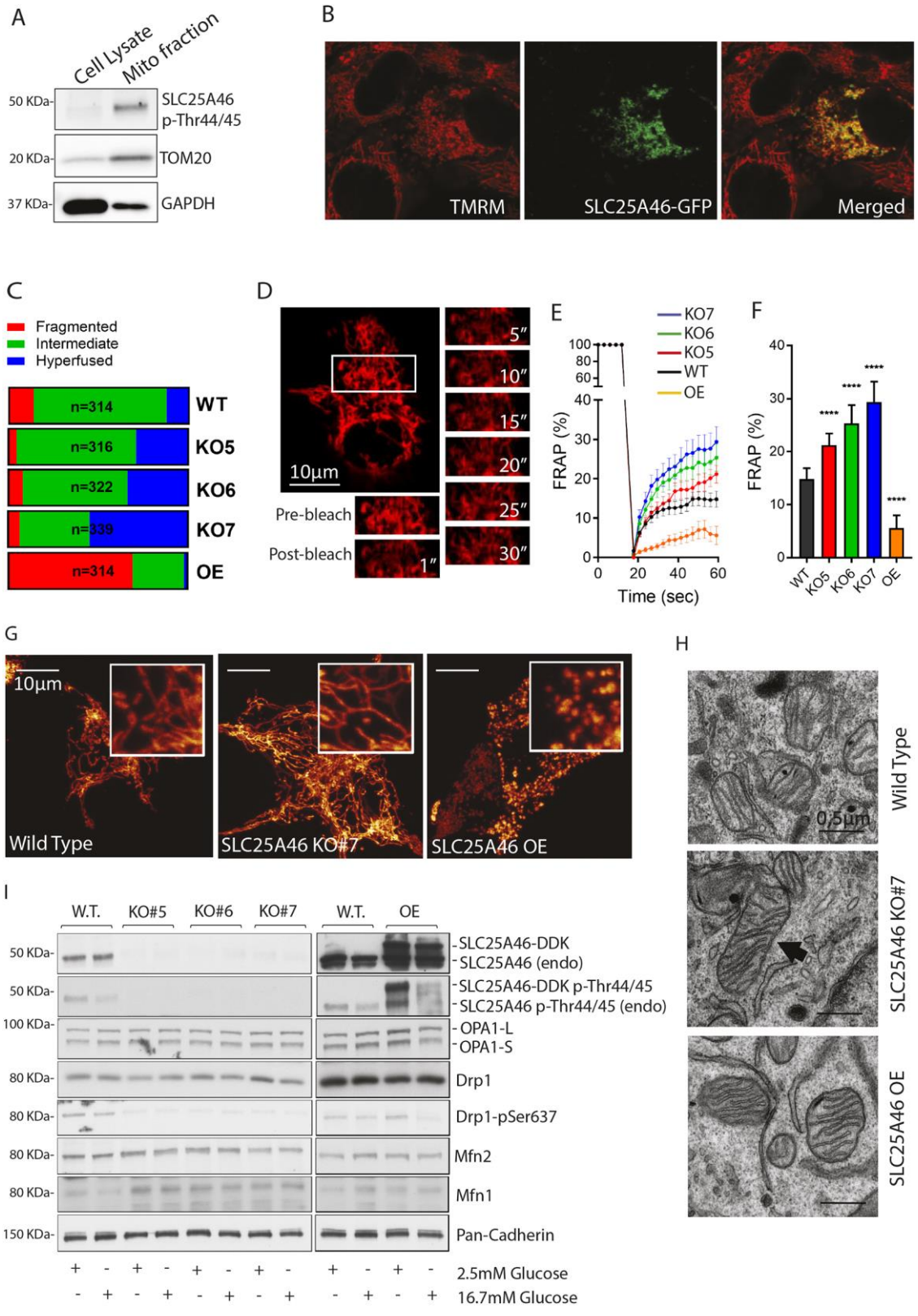

Fig.4. Manipulation of SLC25A46 expression alters mitochondrial dynamics in INS-1E cells. A) Expression of SLC25A46 in total cell lysate and mitochondrial fraction. For comparison the Western blots were also probed for the outer mitochondrial membrane protein TOM20. B) Confocal image of GFP- tagged SLC25A46 (green; middle) and the

mitochondrial dye TMRM (red; left) co-localize (yellow; right). C) Effect of SLC25A46 suppression (K05, K06 and K07 and overexpression (OE) on the percentage of cells displaying fragmented, intermediary or hyperfused mitochondria. D) Representative images of mitochondrially targeted RFP in wild type, SLC25A46 deficient cells (KO#7) and SLC25A46 overexpressing cells (OE). E) Images showing a typical FRAP assay in INS-1E cells expressing mitochondrially targeted RFP. F, G) Fluorescence recovery after photobleaching (F) and fluorescence levels in the bleached area 60 sec after the pulse (G) in wild-type (WT; black), in SLC25A46 deficient clones KO5 (red), KO6 (green), KO7 (blue) and SLC25A46 overexpressing cells (OE; orange). >20 cells analyzed from 3 independent experiments. Average +/-SEM is shown. H) Representative electron microscopy images of the mitochondria ultrastructure in wild type, SLC25A47 deficient (KO#7) and SLC25A46 overexpressing cells. I) Western blot analysis of core mitochondrial shaping proteins in wild type (W.T.), SLC25A46 deficient cells (KO#7) and SLC25A46 overexpressing cells (OE), under basal conditions (2.5 mM glucose) and after short-term glucose (16.7 mM) stimulation. This Western-blot is representative of 3 different biological replicates.

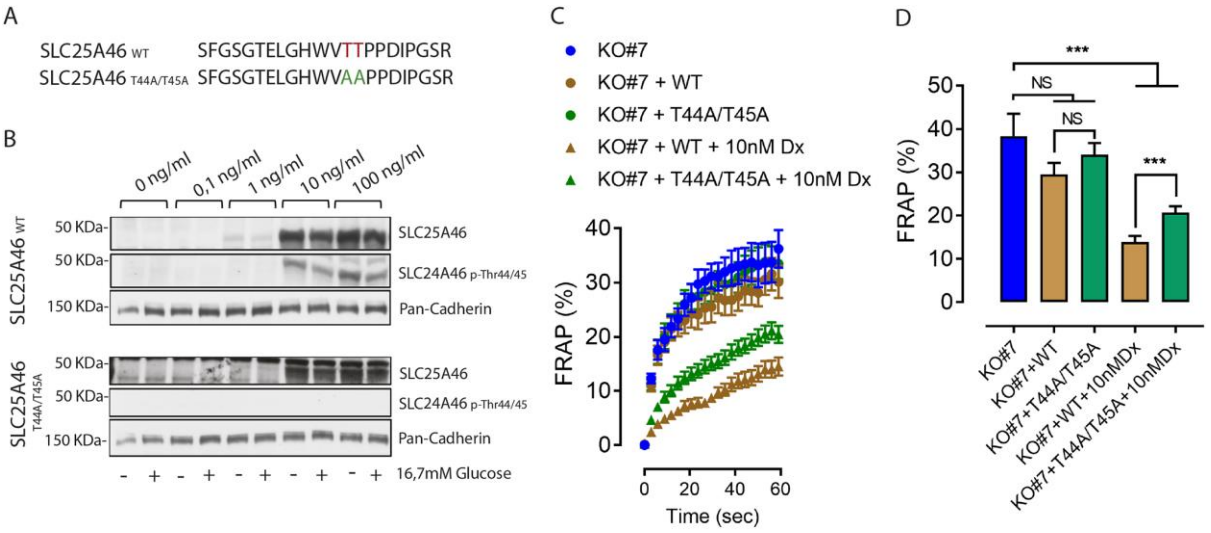

Fig.5. Less pronounced mitochondrial fragmentation following overexpression of an SLC25A46 phosphorylation deficient mutant. A) Peptide sequences of wild type and phospho-null variants (SLC25A46 T44/45A). B) Western blot showing doxycycline-induced expression of wild type and phospho-null variant at different concentrations of doxycycline in INS-1E cell KO7 clone. C) Kinetics of fluorescence recovery after photobleaching in INS-1E KO7 cells (blue) with and without transfection of transgenes indicated in the legend. Control conditions without induction of transgenes (circles). Induction of transgenes with doxycycline (10 nM; triangles). SLC25A46 encoding (brown) and A44/A45 mutant (green) are transfected. D) Fluorescence levels in the bleached area 60 sec after the bleaching pulse. Average of results from 30-40 independent experiments per experimental condition +/- SEM. Color code as in panel C.

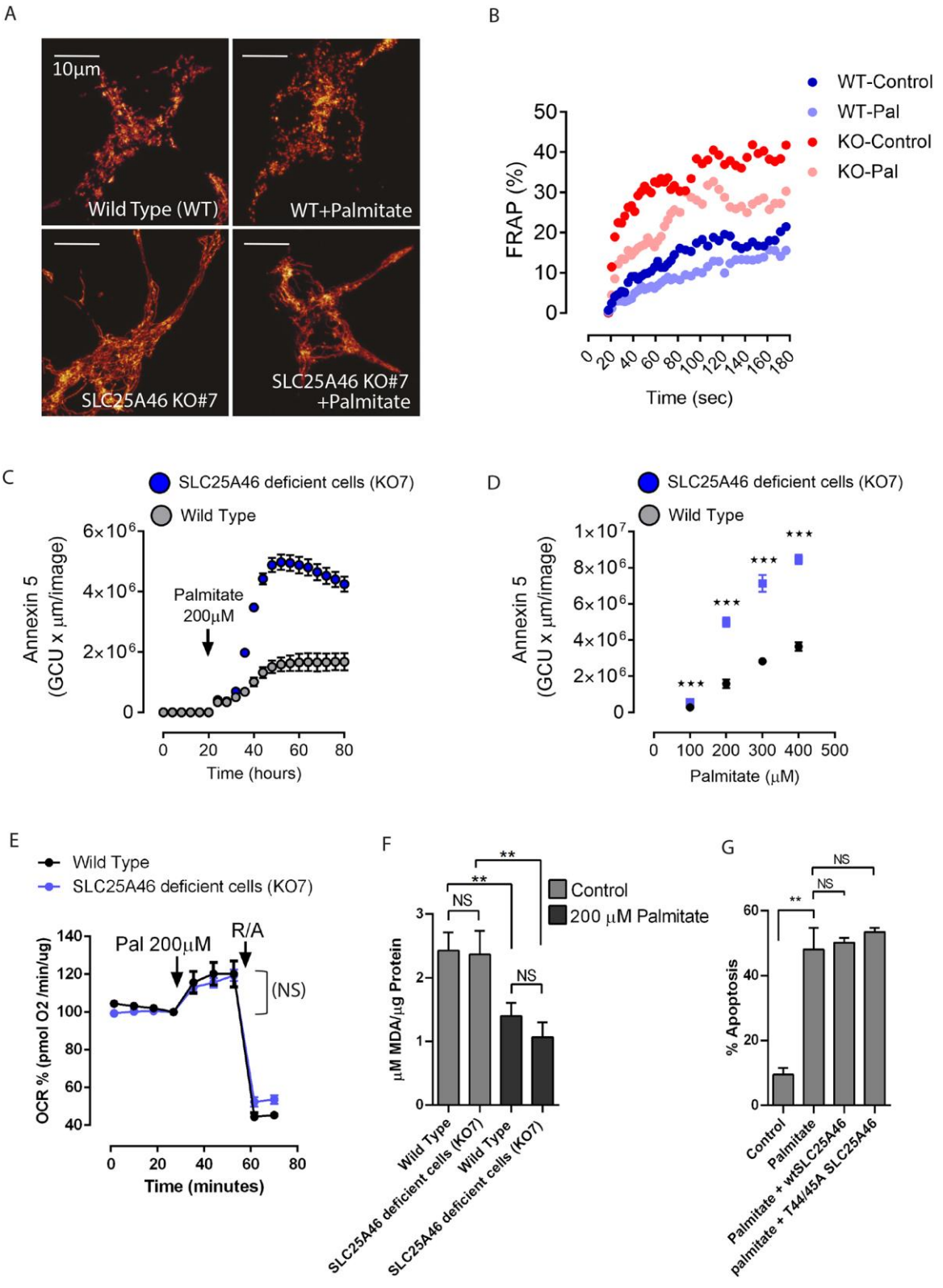

Fig.6. SLC25A46 deficient cells are highly sensitive to palmitate-induced apoptosis. A) Representative images of the mitochondrial networks of cells expressing a mitochondrial-targeted RFP in wild type and SLC25A46 deficient cells (KO#7) treated with and without

200µM palmitate. B) Kinetics of fluorescence recovery after photobleaching of cells expressing a mitochondrial-targeted RFP in in wild type (blue) and SLC25A46 deficient cells (KO#7; red) treated with or without 200 µM palmitate. The paler colors are the conditions treated with palmitate for 24 hours before initiation of the experiment. C) Effect of 200 µM palmitate on apoptosis revealed by Annexin V staining overtime in wild type (grey circles) and SLC25A46 deficient cells (KO#7; blue circles). Shown is the average of 6 measurements +/- SEM from a single experiment. D) Dose response of palmitate on Annexin V staining after 48 hours palmitate incubation of wild type (black circles) and SLC25A46 deficient cells (KO#7; blue squares). Average of 3 independent experiments +/-SEM. E) Effect of palmitate (200 µM), and rotenone/antimycin (1 µM / 1 µg/ml) on oxygen consumption rates in wild type and SLC25A46 deficient cells. Average of results from 3 independent experiments performed in quadruplicate +/- SEM. F) Levels of lipid peroxidation in wild type and SLC25A46 deficient cells incubated either in regular cell culture medium conditions or under the same regular control condition but supplemented with palmitate 200 µM for 48 hours. G) Effect of 200 µM palmitate on apoptosis revealed by Annexin V, in control cells or expressing either wild type SLC25A46 or the phospho-null variant (SLC25A46 T44/45A).

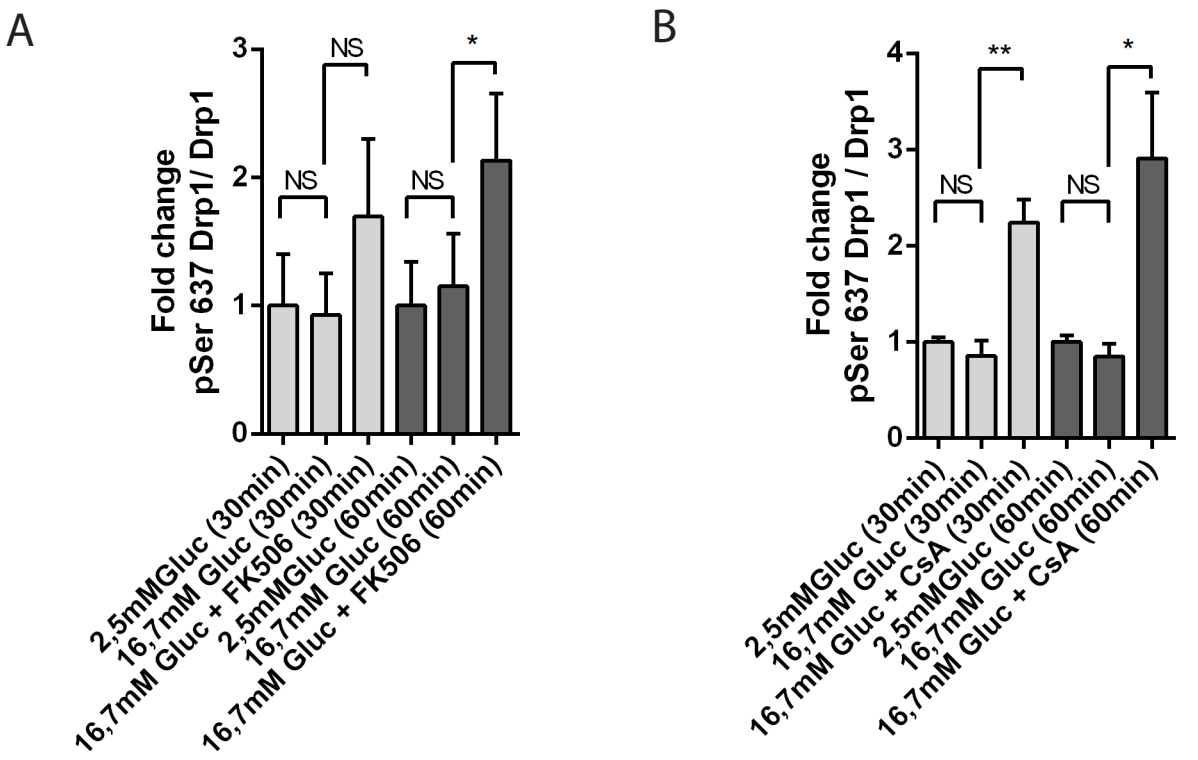

Fig. S1. Effect of glucose stimulation and calcineurin inhibitors on Ser 637-Drp1 phosphorylation status. A) Graph bars show quantification of 637-Drp1 phosphorylation status upon 16,7 mM glucose and 30 µM FK506 incubation from western-blot experiments displayed in Fig. 2D. Average of 4 independent experiments (N=4) +/- SEM. B) Graph bars show quantification of 637-Drp1 phosphorylation status upon 16,7mM glucose and 50µM CsA incubation from western-blot experiments displayed in Fig. 2D. Average of 4 independent experiments (N=4) +/- SEM.

SLC26A46 KO#5

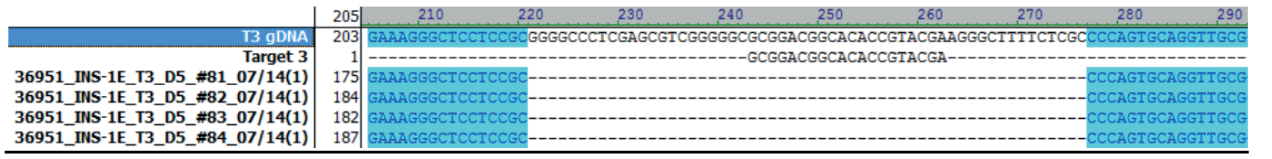

SLC26A46 KO#6

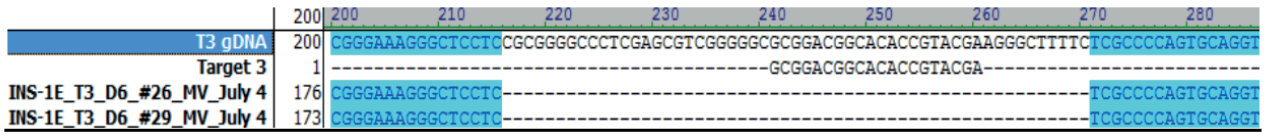

SLC26A46 KO#7

Fig. S2. Knock-out clones sequencing confirmed successful genome editing. KO#5, KO#6 and KO#7 have shown a 56bp deletion, a 55bp deletion, and a 38bp deletion respectively that induce frame shift mutations.

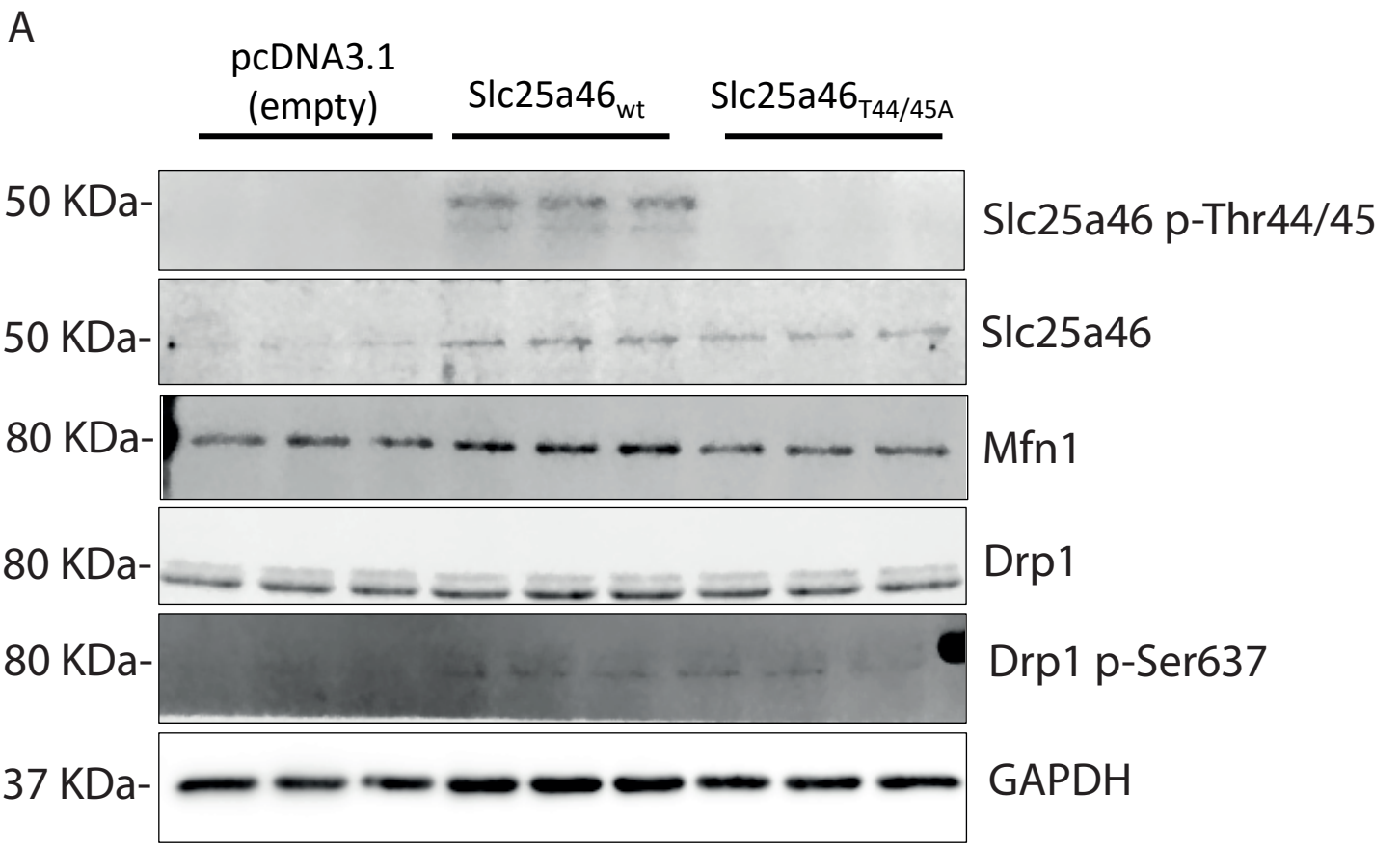

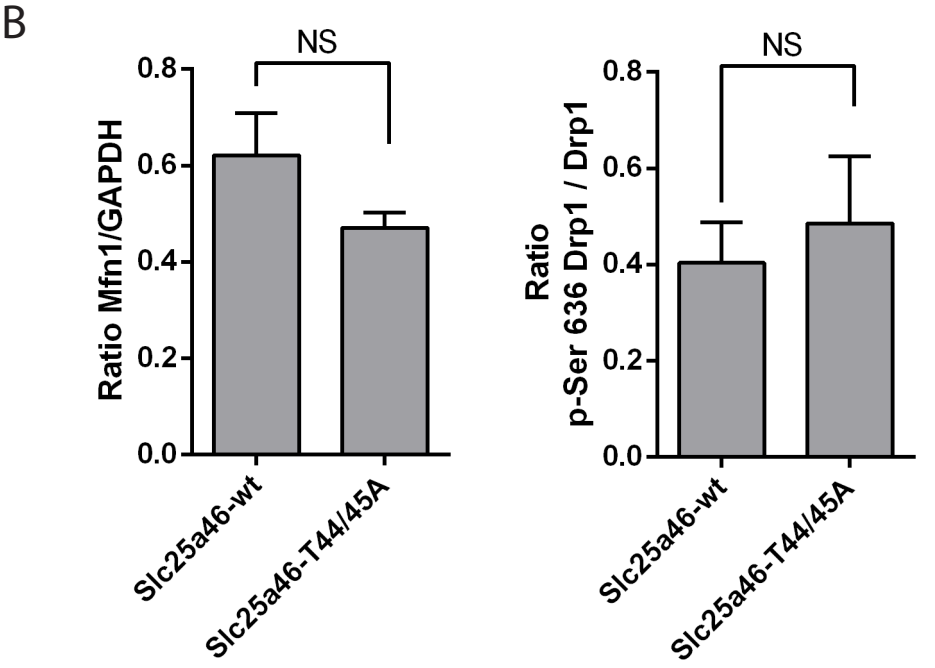

Fig. S3. Thr44/45 phosphorylation status does neither impacts Mfn1 levels nor Ser637-Drp1 phosphorylation. A) Western blot analysis of Mfn1, Drp1 and p-Ser-636 Drp1 phosphorylation levels in SLC25A46 deficient cells (KO#7) overexpressing either wild type or the phospho-null variant (SLC25A46 T44/45A). B) Bar graphs showing the Western-blot quantification. Effect of wild type and phospho-null variants on Mfn1 expression and p-Ser-636 Drp1 phosphorylation levels. Average of 3 independent experiments (N=3) +/- SEM.

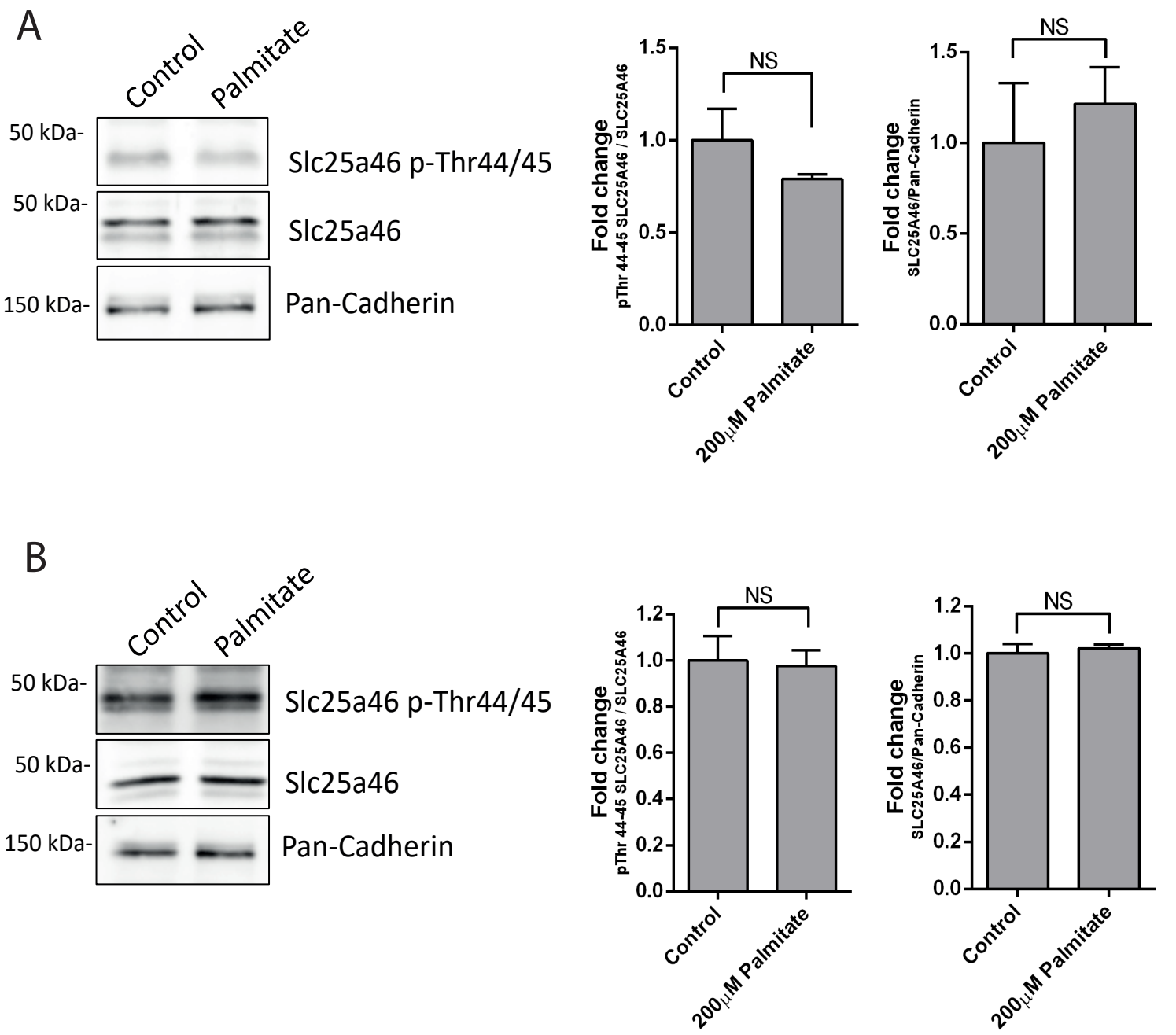

Fig. S4. Effect of acute and chronic 200µM palmitate incubation on Thr44/45 phosphorylation status and SLC25A46 levels. A) Western blots showing the effect of 60 min incubation with 200µM palmitate on SLC25A46 expression and Thr44/45 phosphorylation levels. Graph bars show Western-blot quantification. Average of 3 independent experiments (N=3) +/- SEM. B) Western blots showing the effect of 48 hours incubation with 200µM palmitate on SLC25A46 expression and Thr44/45 phosphorylation levels. Graph bars show Western-blot quantification. Average of 3 independent experiments (N=3) +/- SEM.

Table S1. Excel sheet displaying the list of mitochondrial peptides whose phosphorylation status was significantly altered upon 5 minutes of glucose stimulation. The list provides information on gene name, uniport ID, full name, peptide sequence, phospho-site, fold change induced by glucose stimulation and p-values.

Mitominer output (Gene name)	Entry (Uniprot ID)	Entry name	Phospho peptide	P-Site	Fold change (log2)	p-value
Sphkap	F1LNS0	SPKAP_RAT	ETSACHNAVALKSPR	S1399	-0,658176667	0,00965116
Slc25a46	Q5EB62	S2546_RAT	SFGSGTELGHWVTTPPDIPGSR	T45	-0,2975125	0,05624512
Bad	O35147	BAD_RAT	SAPPNLWAAQR	S137	-0,0933	0,00579181
Sphkap	F1LNS0	SPKAP_RAT	IIADDGEAANASPGPVSGGSPSQVEK	S1323	-0,0901822	0,02510845
Mief1	Q5XIS8	MID51_RAT	AISAPTSPTR	S59	0,1027854	0,00559878
Armc10	B1WBW4	ARM10_RAT	SAEDLTEGSYDAILSAEQLEK	S43	0,1378198	0,00213998
Sphkap	F1LNS0	SPKAP_RAT	NPLHTLSYDSSEQR	S828	0,1850348	0,01303723
Shc1	F1LN14	SHC1_RAT	ELFDDPSYVNIQNLDK	Y313	0,1968048	0,01982353
Sphkap	F1LNS0	SPKAP_RAT	ASSSGLCKSDSCLYR	S1269	0,2181028	0,00112775
Dnmt1	F1LQT9	DNMT1_RAT	SKSDSETMIEASSSSVATR	S142	0,2533735	0,03977016
Sphkap	F1LNS0	SPKAP_RAT	SNSLLESTDYWLQNQR	S50	0,3033124	0,00037116
Raf1	P11345	RAF1_RAT	DAVFDGSSCISPTIVQQFGYQR	S29	0,3876882	0,00022799
Elac2	G3V6F5	RNZ2_RAT	AALLTQQADSSEDREPHQK	S801	0,486004	0,01558629

Table S2. Excel sheet displaying the list of mitochondrial peptides whose phosphorylation status was significantly altered upon 30 minutes of glucose stimulation. The list provides information on gene name, uniport ID, full name, peptide sequence, phospho-site, fold change induced by glucose stimulation and p-values.

Mitominer output (Gene name)	Entry (Uniprot ID)	Entry name	Phospho peptide	P-Site	Fold change (log2)	p-value
Sphkap	F1LNS0	SPKAP_RAT	ETSACHNAVALKSPR	S1399	-0,590943333	0,02239091
Slc25a46	Q5EB62	S2546_RAT	SFGSGTELGHWVTTPPDIPGSR	T45	-0,5606475	0,003000221
Cluh	D3ZKG9	D3ZKG9_RAT	ALEGMGSPQTAK	S1335	-0,13982	0,01848435
Bckdk	Q00972	BCKD_RAT	STSATDTHHVELAR	S33	-0,0937172	0,034863404
Sphkap	F1LNS0	SPKAP_RAT	EECVGESETLLPQSGSLEEAEGPQPEETIPDVAR	S1435	-0,03355	0,046679911
Acly	G3V888	ACLY_RAT	AKPAMPQDSVPSPR	S481	0,0498092	0,025667772
Stat3	P52631	STAT3_RAT	FICVTPTTCSNTIDLPMSPR	S727	0,0574556	0,049421833
Armc10	B1WBW4	ARM10_RAT	SAEDLTEGSYDAILSAEQLEK	S43	0,0748682	0,039765618
Dnmt1	F1LQT9	DNMT1_RAT	SKSDSETMIEASSSSVATR	S140	0,1059882	0,002213593
Dnmt1	F1LQT9	DNMT1_RAT	EADEDEEADDDIPELPSPKK	S718	0,1377595	0,008486194
Hspd1	P63039	CH60_RAT	TVIIEQSWGSPK	S70	0,14835	0,001440016
Sphkap	F1LNS0	SPKAP_RAT	SNSLLESTDYWLQNQR	S50	0,1957494	0,018347707
Bckdk	Q00972	BCKD_RAT	STSATDTHHVELAR	S31	0,199944333	0,03284795
Raf1	P11345	RAF1_RAT	DAVFDGSSCISPTIVQQFGYQR	S29	0,2394098	0,00144226
Sphkap	F1LNS0	SPKAP_RAT	QSSTESITEEFYK NDHLNVRPSCPSKQSSTESITEEFYK	S1167	0,271517	0,028907797
Elac2	G3V6F5	RNZ2_RAT	NMQASPAPAEK	S469	0,291997667	0,008269831
Akap1	D4A9M6	AKAP1_RAT	RRSESSGNLPSIVDTR	S101	0,29396825	0,003085912
Elac2	G3V6F5	RNZ2_RAT	AALLTQQADSSEDREPHQK	S800	0,430345333	0,018741954

Table S3. Excel sheet displaying the list of mitochondrial peptides whose phosphorylation status was significantly altered upon 60 minutes of glucose stimulation. The list provides information on gene name, uniport ID, full name, peptide sequence, phospho-site, fold change induced by glucose stimulation and p-values.

Mitominer output (Gene name)	Entry (Uniprot ID)	Entry name	Phospho peptide	P-Site	Fold change (log2)	p-value
Slc25a46	Q5EB62	S2546_RAT	SFGSGTELGHWVTTPPDIPGSR	T45	-0,77465	0,00264335
Sphkap	F1LNS0	SPKAP_RAT	ETSACHNAVALKSPR	S1399	-0,54717	0,00291344
Fundc1	Q5BJS4	FUND1_RAT	NPPPQDYESDDESYEVLDLTEYAR	S17	-0,31592	0,02499702
Bad	O35147	BAD_RAT	SAGTATQMR	S171	-0,27376	0,03252597
Sphkap	F1LNS0	SPKAP_RAT	IIADDGEAANASPGPVSGGSPSQVEK	S1323	-0,24371	0,03959347
Sphkap	F1LNS0	SPKAP_RAT	KDAVTEGNCSPVSSPSK DAVTEGNCSPVSSPSK	S1365	-0,19495	0,01787232
Stat3	P52631	STAT3_RAT	FICVTPTTCSNTIDLPMSPR	T714	-0,15846	0,0425411
Bad	O35147	BAD_RAT	RMSDEFEGSFK	S156	-0,13301	0,01927135
Bad	O35147	BAD_RAT	SAPPNLWAAQR	S137	-0,1105	0,04480676
Hnrnpk	Q5D059	HNRPK_RAT	RDYDDMSPR DYDDMSPR	S284	0,050123	0,0369475
Acly	G3V888	ACLY_RAT	AKPAMPQDSVPSPR	S481	0,076326	0,00882381
Uba1	Q5U300	UBA1_RAT	RVSGPDPKPGSNCSSAQSVLSEVSSVPTNGMAK	S13	0,099595	0,03738047
Akap1	D4A9M6	AKAP1_RAT	RSESSGNLPSIVDTR	S103	0,121388	0,00394637
Mief1	Q5XIS8	MID51_RAT	AISAPTSPTR	S59	0,142664	0,00787807
Elac2	G3V6F5	RNZ2_RAT	AALLTQQADSSEDREPHQK	S801	0,206217	0,00460782
Akap1	D4A9M6	AKAP1_RAT	RRSESSGNLPSIVDTR	S101	0,236943	0,01108012
Akt1	P47196	AKT1_RAT	SGSPSDNSGAEEMEVALAKPK	S126	0,240758	0,00940459
Slc9a6	D3ZJ86	D3ZJ86_RAT	LVLPMDDSEPALNSLDDTRHSPA	S700	0,265696	0,02655677
Fundc1	Q5BJS4	FUND1_RAT	NPPPQDYESDDESYEVLDLTEYAR	Y18	0,292689	0,01573256
Elac2	G3V6F5	RNZ2_RAT	AALLTQQADSSEDREPHQK	S800	0,29987	0,02207418
Raf1	P11345	RAF1_RAT	DAVFDGSSCISPTIVQQFGYQR	S29	0,412483	0,0038409